

11102-CR

57128

p.56

Department of Aerospace Engineering
The Pennsylvania State University
University Park, PA 16802

**ANALYSIS AND DESIGN OF PLANAR AND NON-PLANAR WINGS
FOR INDUCED DRAG MINIMIZATION**

ANNUAL PROGRESS REPORT

NASA Grant NAG-1-1198

**ATTN: Raymond E. Mineck
Technical Monitor**

K. Mortara, Dennis M. Straussfogel, and Mark D. Maughmer

**Department of Aerospace Engineering
The Pennsylvania State University
University Park, PA 16802**

December 1991

**(NASA-CR-189509) ANALYSIS AND DESIGN OF
PLANAR AND NON-PLANAR WINGS FOR INDUCED DRAG
MINIMIZATION Annual Progress Report
(Pennsylvania State Univ.) 56 p CSCL 01A**

N92-13999

**Unclas
63/02 0057128**

Table of Contents

	Page
I. Summary	1
II. Introduction	2
III. Background Discussion	4
Lifting-Line Theory (Prandtl-Lanchester)	4
Modified Lifting-Line Theory (Eppler)	5
Vortex-Lattice Methods	6
Linear Panel Methods	7
Full Potential, Euler and Navier-Stokes Methods	8
A Note on Calculating the Deformed Wake Shape	9
IV. The Development of a Method for the Aerodynamic Design and Analysis of Planar and Non-Planar Wings	10
Panel Method Solution	10
Induced Drag Calculation	11
Extrapolation Factor	11
V. Validation Using Computed Results	13
Extrapolation Factor	13
Other Computational Methods	14
<i>Pressure Integration</i>	14
<i>Trefftz Plane Method</i>	15
<i>Modified Lifting Line</i>	15
Comparison of Results	16
VI. Validation Using Experimental Results	17
Description of Test Model	17
Prediction Method	17
Presentation and Discussion of Results	18
VII. Discussion of Design Tools for Planar and Non-Planar Wings Having Minimum Induced Drag	21
VIII. Conclusions and Recommendations	24
IX. References	26
Table	28
Figures	29

I. Summary

The goal of the work reported herein is to develop and validate computational tools to be used for the design of planar and non-planar wing geometries for minimum induced drag. Because of the iterative nature of the design problem, it is important that, in addition to being sufficiently accurate for the problem at hand, they are reasonably fast and computationally efficient. Toward this end, a method of predicting induced drag in the presence of a non-rigid wake has been coupled with a panel method. The induced drag prediction technique is based on the Kutta-Joukowski law applied at the trailing edge. Until recently, the use of this method has not been fully explored and pressure integration and Trefftz-plane calculations favored. As is shown in this report, however, the Kutta-Joukowski method is able to give better results for a given amount of effort than the more common techniques, particularly when relaxed wakes and non-planar wing geometries are considered. Using these tools, a workable design method is in place which takes into account relaxed wakes and non-planar wing geometries. It is recommended that this method be used to design a wind-tunnel experiment to verify the predicted aerodynamic benefits of non-planar wing geometries.

II. Introduction

Improvement in the aerodynamic efficiency of commercial transport aircraft will reduce fuel usage with subsequent reduction in both monetary and environmental costs. To this end, the current research is aimed at reducing the overall drag of these aircraft with specific emphasis on reducing the drag generated by the lifting surfaces. The ultimate goal of this program is to create a wing design methodology which will optimize the geometry of the wing for lowest total drag within the constraints of a particular design specification. The components of drag which must be considered include profile drag, induced drag, and wave drag. The optimization problem is that of assessing the various parameters which contribute to the different components of wing drag, and determining the wing geometry which will generate the best overall performance for a given aircraft mission.

The primary thrust of the research effort to date has concentrated on the prediction and minimization of induced drag. Recently reported findings have indicated that induced drag may be reduced by utilizing unconventionally shaped and/or non-planar wing planforms¹⁻³. To investigate these findings, it is necessary to be able to predict induced drag with reliability and precision. Furthermore, if the same method is to be used for design purposes then, because of the iterative nature of the design process, it is also necessary that the method be computationally efficient. Toward this end, an analysis method has been developed which has the accuracy of a higher-order panel method using a large panel density while requiring only 2 percent of the computation time. The technique is capable of accounting for the effects of a free wake in the prediction of the induced drag for both planar and non-planar wings.

At this point, the newly developed method for predicting induced drag has been validated by comparing its predictions with those of other commonly used analysis schemes. It has also been used to match the experimental results of a recent wind-tunnel test directed at exploring the influence of planform geometry on induced drag. In both exercises, the new method performed very well. Currently, it is being used to study the trade-off

between induced drag and profile drag in the design of non-planar wings in which the total drag is minimized. If these studies indicate that significant aerodynamic gains are possible through the use of non-planar wing geometries, then this induced-drag analysis method should be extremely useful to the overall design problem considering such things as structural weight, total span, wing-root bending moment, and so forth. It is only at this point that wing geometries having reduced induced drag can be used to advantage in the design of more efficient aircraft.

III. Background Discussion

To calculate the induced drag generated by a lifting surface it is required that all, or at least part, of the velocity field be determined in the vicinity of the wing. Linear potential flow methods generally solve for the velocity over only a small part of the flow field and thus save a tremendous amount of computation time. The induced drag is calculated in these methods by either applying the Kutta-Joukowski law to the bound vorticity, or by integrating the streamwise component of pressure on the surface of the wing. In this way potential flow methods require solution of the velocity field only at points defining the idealized lifting surface as opposed to points defining the entire flow field. The potential flow methods which employ the Kutta-Joukowski law determine the downwash velocity at the wing either by direct calculation or by analyzing the flow in the far-wake where the flow is assumed to be two-dimensional (i.e., in the Trefftz plane), and relating that solution to the flow at the wing. The latter technique assumes the wake of the wing to be rigid and aligned with the free-stream velocity. A more computationally intensive approach for calculating the induced drag is to solve the governing equations over the entire "region of influence" in the flow field. The induced drag is then determined by integrating the resulting distributed pressure force on the wing surface, or directly from the calculated vorticity shed into the wake. The amount of computer time required to solve the governing equations makes this approach impractical as a tool for preliminary design.

The following is a brief explanation of available methods for calculating induced drag and a discussion of the strengths and weaknesses of the potential flow methods, as well as methods which numerically solve the Euler or Navier-Stokes equations.

Lifting-Line Theory (Prandtl-Lanchester)

The lifting-line theory of Prandtl analyzes the flow field as a potential field with the wing modeled as a singularity in the form of a line vortex of varying strength located at the wing quarter-chord point¹. Helmholtz's theorem requires that the spanwise change in

vorticity of the lifting line be shed into a sheet of distributed trailing vorticity. The trailing vorticity is assumed to be aligned with the free-stream velocity and to extend downstream to infinity. The strength of the trailing vortex sheet at any point is equal to the spanwise change in vortex strength at the corresponding point on the lifting line. In this model, the sheet of trailing vorticity is assumed to be rigid and does not deform under its own induced velocity. The velocity that the trailing vortex sheet induces on the lifting line is used to calculate the induced drag of the wing.

Munk made use of the lifting-line theory to calculate the optimum spanwise lift distribution for minimum induced drag within the context of the given assumptions⁵. In this case, the minimum induced drag is achieved when the induced velocity normal to the lifting line is proportional to the cosine of the local dihedral angle. For a straight lifting line (dihedral angle equal to zero everywhere along the span) the lift distribution that generates this induced velocity distribution is elliptical. For a curved lifting line, which models a non-planar wing with spanwise varying dihedral angle, the optimum lift distribution for minimum induced drag is well defined, again, within the limits of the modeling assumptions⁶. Several questions arise, however, regarding the assumptions used in obtaining these results. In particular, the lifting-line model ignores the effect of the chordwise distribution of vorticity on the downwash distribution since it collapses all the vorticity generated at a given spanwise location to a single point. Also, the effect that the deforming wake might have on wing performance is neglected. While lifting-line theory is useful for approximating the performance of unswept large-aspect-ratio wings, once the chord distribution is fixed, the method is unable to account for any differences between wings due to planform shape.

Modified Lifting-Line Theory (Eppler)

A recent modification to lifting-line theory locates the lifting line at the trailing edge of the planform instead of along the quarter-chord line⁷. As in the Prandtl lifting-line model, the effects of chordwise loading are not included; however, the influence of the trailing-edge shape is now taken into account. It is assumed in this method that the bound vorticity does

not influence the induced velocity in either the wake or at the lifting line and is therefore not considered in any downwash calculations. Induced drag is calculated in this method by applying the Kutta-Joukowski law to the bound vorticity at the trailing edge. The Eppler method can be implemented with either fixed- or free-wake analysis, and can consider planar and non-planar wing planforms. The advantage of the method is that it possesses the simplicity of the Prandtl lifting-line model, but includes some planform effects in the form of the trailing-edge shape. Intuitively, the Eppler model makes sense in that it places the bound vortex line at the location where the vorticity is actually shed into the flow.

Vortex-Lattice Methods

The vortex-lattice method⁸ uses an array of horseshoe vortices with spanwise segments bound to the wing and streamwise segments trailing downstream from the trailing edge parallel to the free-stream velocity. The strength of each vortex is determined by satisfying the condition that the flow be tangent to the mean camber line of the wing at a number of control points equal to the number of vortices used. This constraint defines a system of simultaneous linear equations which are solved for the vortex strengths. The strengths of the streamwise trailing vortex filaments are taken as the sum of the strengths of the horseshoe vortices distributed over the chord at a given spanwise position.

Modeling the wing as a lattice of vortices attempts to capture the effect of the chordwise loading on the overall wing aerodynamics. The vortex-lattice method does not capture any thickness effects in that it models the wing as a set of discrete line vortices located on the mean camber line. The traditional vortex-lattice method also does not account for the influence of the free wake. Typically the wing wake is modeled as straight, non-deforming vortex filaments aligned with the free stream; however, the effect of the deforming wake can be included in this method using wake relaxation⁹.

Induced drag is normally calculated in the vortex-lattice method by applying the Kutta-Joukowski law on the spanwise bound vortex segments under the influence of the local downwash. Consequently, the orientation of the bound vortices is important and

some research has been done regarding the way in which the lattice is constructed¹⁰⁻¹³. One question which arises is whether the spanwise vortex segments should be aligned perpendicular to the free-stream velocity, aligned with the sweep angle of the wing, or aligned in some other direction depending on the wing planform shape. Unfortunately, it is found that the choice of lattice shape can have a significant effect on the solutions obtained with this formulation.

Linear Panel Methods

Panel methods discretize the wing upper and lower surfaces into source, doublet, or vortex panels which induce a perturbation on the uniform (free-stream) velocity field¹⁴. Unlike vortex-lattice methods, such methods take the effects of wing thickness into account. Low-order panel methods assume the panels to be flat and have constant source, doublet, or vortex strength over the entire panel¹⁵, while higher-order methods consider surface curvature and source, doublet, or vortex strength derivative effects. The strength of each panel is determined by satisfying the flow tangency condition at a number of control points equal to the number of panels used. As in the vortex-lattice method, the application of the appropriate boundary conditions produces a system of linear simultaneous equations that can be solved for the panel strengths. The shape of the freely deforming wake can also be computed by discretizing the wake into panels and calculating the flow velocity at each panel. The wake is then reoriented so that each panel is aligned with the local velocity vector. Since the strength and orientation of the panels in the wake effect those on the wing, this process must be iterated until it converges to a steady-state wake shape.

For panel methods, induced drag can be calculated by taking the streamwise component of the product of surface pressure and panel area summed over all the wing panels. This method is extremely sensitive to errors in the calculated pressure distribution which are most pronounced near the leading edges and wing tips, even in higher-order methods³. Another means of calculating induced drag is to either assume a rigid wake, or attempt to compute the deformed wake shape, then numerically integrate over the velocity field far

downstream where the flow is assumed to be two-dimensional. In the relaxed-wake case, this is extremely difficult in that it is as yet not possible to resolve velocities well enough in the cores of the rolled-up trailing vortex sheet to accurately predict the induced drag.

Full-Potential, Euler and Navier-Stokes Methods

Linearized potential flow methods do not include the effects of compressibility and are therefore inadequate for the transonic wing design problem. To handle these effects in calculating induced drag, a numerical solution of at least the full potential or Euler equations is required. The solution must be found over a large enough region of the flow so as to capture the significant upstream and downstream effects on the wing performance. As in the linearized case, the full-potential equations require that the wake geometry be specified, or fitted, as a boundary condition before solution takes place¹⁶. In the case of the Euler equations, the freely deforming wake shape is captured in the solution. Once the velocity distribution on the wing is determined, the lift and induced drag on the wing can be found from a surface pressure integration similar to that used in panel methods. Determining lift and drag from a far-field wake-integration scheme has also been attempted¹⁷.

It should be noted that even though the Euler equations do not contain any viscosity terms, the numerical solution shows some viscous-like behavior because of the truncation error incurred in the finite-differencing process. By decreasing the gradients in the solution, this *artificial viscosity* will drive the mathematical solution in the same direction, but not necessarily to the same extent, as the real viscous effects. Consequently, the far-field wake-integration methods for determining induced drag may be subject to errors brought on by a non-physical wake shape.

In order to numerically solve the Euler equations for a simple wing geometry over the number of grid points needed for reasonable accuracy, approximately 3 hours of computation time on a Cray Y-MP is required¹⁷. It is expected that the solution to the full-potential equation would require a similar effort¹⁸. This amount of computation time would be generally considered excessive for use in an iterative design process.

To include both the effects of viscosity and compressibility in the wing design problem, either a boundary layer solution or the full Navier-Stokes equations must be used. Numerically solving the Navier-Stokes equations requires an amount of computation time greater than that required for solving the Euler equations. Thus, this approach is also impractical for routine design activity.

A Note on Calculating the Deformed Wake Shape

Due to the mathematical instability inherent in the self-induced motion of a vortex sheet, accurate determination of the shape of a freely deforming wake in any potential flow technique is an extremely difficult problem. The wake relaxation method calculates the local velocity at points in the wake, aligns the trailing vortex filaments with the local velocity (streamlines), then iterates until convergence to a steady state wake shape is achieved⁰. A time-stepping method used in conjunction with some vortex-lattice¹⁰ and panel²⁰ methods convects the shed vortex filaments with the instantaneous local velocity. This method is suited for unsteady flow problems whereas the wake-relaxation method assumes steady-state conditions exists. Still another scheme treats the wake as an array of two-dimensional point vortices moving in planes perpendicular to the free-stream velocity²¹. Precise analysis of deforming vortex sheets has been attempted recently and it has been noted that even for a simple two-dimensional vortex sheet problem "the calculation of the self-induced motion of vortex sheets has proved quite intractable and has resisted the best efforts of numerous investigators."²² Based on these findings, it should be noted that the calculated shape of the deformed wake, regardless of the method used, may vary significantly from reality. If the influence of the wake shape on the induced drag is not significant, however, then the difference between the shape of the actual wake and that modeled is not critical to the design of optimum wing geometries. This issue will be addressed in the following sections.

IV. The Development of a Method for the Aerodynamic Design and Analysis of Planar and Non-Planar Wings

After considering all of the methods described, it was concluded that none had the speed and accuracy required to be effective as a tool for designing wings having minimum induced drag. Thus, a hybrid method was created to capture the best features of several of the methods. The hybrid method combines the lift distribution and wake relaxation of a low-order panel method with the induced drag calculation of the modified lifting-line method. In addition, the panel method solution is iterated, to take into account the changing influence of the deforming wake. Furthermore, the method is reasonably fast and retains sufficient accuracy to be useful for design work.

Panel Method Solution

The first element of the hybrid method is a low-order panel method which models the wing with flat panels each having a constant distributed source and doublet strength. The maximum number of panels that the code can handle is limited only by the available machine memory. A wake relaxation scheme is used with the vorticity shed from a given point on the trailing edge taken as the difference in doublet strengths of the upper and lower surface panels which join to form the trailing edge at that point.

The strengths of the wing panels are first solved using a fixed wake aligned with the free-stream velocity vector. Given this distribution of sources and doublets on the wing, with trailing wake vortex filaments of corresponding strength, the wake is then relaxed to align itself with the local velocity vectors (streamlines) generated by the source, doublet, and vortex distribution. This wake relaxation is an iterative process and usually converges within three iterations.

Once the wake shape is determined, the induced drag is calculated by means of a method to be described shortly. Using the deformed wake shape, which now has an influence on the wing different from that of the previously assumed flat, fixed wake, the panel

method is resolved, generating a new distribution of source and doublet strengths over the wing. With the new source, doublet, and corresponding vortex filaments strengths, the wake is further relaxed to a new shape, the induced drag recalculated, and the process continued until convergence, based on the induced drag calculation, is achieved.

Induced Drag Calculation

The induced drag is calculated in the hybrid method by application of the Kutta-Joukowski law

$$\vec{F} = \vec{V} \times \vec{\Gamma}$$

at the trailing edge of the wing. The velocity in this equation is the velocity normal to the free-stream velocity induced by the wake vortex filaments, excluding the influence of the wing source and doublet distribution. This is an extension of the assertion by Munk⁵ that the bound vorticity need not be included in the calculation of induced downwash because the influence from the transverse vortices of any two “lifting elements” is reciprocal and cancelling. Although Munk’s formulation was developed assuming a fixed wake, the influence of the bound vorticity is unaffected by what is happening downstream, and therefore this assertion should be equally valid whether the wake is fixed or free to deform. The wake shape used in this induced drag calculation is, of course, that found from the preceding panel method solution. After the induced drag is calculated, the panel method is resolved and, using the new wake shape, the induced drag recalculated. This process is continued until convergence is achieved based on the change in the calculated induced drag from one iteration to the next.

Extrapolation Factor

An important element of the present method is an extrapolation factor which all but eliminates the dependence of the computed induced drag on the spanwise number of panels used in modeling the wing. This factor is a function of the number of spanwise panels and

is calculated by comparing the induced drag computed using the lifting-line part of the hybrid method with a fixed wake to that computed analytically for an elliptically loaded wing. Specifically, the extrapolation factor is found by applying the Kutta-Joukowski law at the trailing edge of an elliptically loaded wing using the velocity induced by a flat, fixed wake modeled with a given number of trailing vortex filaments. The strengths of the trailing filaments are equal to the spanwise derivative of the bound vorticity. As the span efficiency for this case is known analytically to be unity, the span efficiency computed by the above method can be used as an extrapolation factor for any results computed using the same number of spanwise increments. It will be shown that the effect of the extrapolation factor is to dramatically reduce the number of wing panels needed for accurate drag determination. This results in a significant reduction in required computation time.

V. Validation Using Computed Results

The hybrid panel/trailing-edge method has been validated by testing its robustness, evaluating its self-consistency, and comparing results obtained using it to those from other computational methods.

The span efficiency factor, e , was calculated using several methods for wings with varying amounts of sweep. The wing geometries used all have elliptical chord distributions and use an NACA 0012 airfoil. The location of the trailing edge of the wing geometries is defined by the equation

$$x_{t,e} = c_{root} \left[\left(\frac{x_{tip}}{c_{root}} \right) (1 - \sqrt{1 - \eta^2}) + \sqrt{1 - \eta^2} \right]$$

where η is the non-dimensional span location, and the tip location (x_{tip}) relative to the root chord varies from $0.25c_{root}$ to $1.50c_{root}$. The aspect ratio of the geometries analyzed is 7.00. Although the hybrid code can analyze models with both twist and dihedral, neither was included in the validation test runs. The test geometries which have relative tip locations from 0.25 (unswept elliptical) to 1.50 (full crescent) are shown in Fig. 1.

Extrapolation Factor

The extrapolation factor discussed in the previous section is presented as a function of the number of spanwise increments in Fig. 2. Fig. 3 shows the effect of using the extrapolation factor on the calculated value of the span efficiency factor, e . With no extrapolation factor included, e varies significantly as a function of the spanwise panel density as shown by the uncorrected curves. For spanwise panel numbers greater than 20, e becomes essentially independent of panel number when use is made of the extrapolation factor. This result will be further demonstrated by comparison to a higher order panel method in the following sections.

With respect to the number of chordwise panels necessary for accurate induced drag calculations, as demonstrated in Fig. 4, the value of e is seen to be relatively insensitive

to the number of chordwise panels provided at least 50 panels (25 upper surface, 25 lower surface) are used.

Other Computational Methods

The results from the hybrid panel/trailing-edge method have been compared to those from several other drag prediction methods. A brief description of these methods follows.

Pressure Integration

The most direct way to predict induced drag using a panel method is by summing the streamwise component of the predicted surface pressure force over all of the wing panels. Since the mathematical model used in a panel method does not account for viscous effects, the streamwise force thus computed is the induced drag. It has been shown^{2,3} that the induced drag calculated in this way is extremely sensitive to the panel density in both the spanwise and chordwise directions. This is the major shortcoming of this prediction method in that to obtain reasonably consistent results, a large number of surface panels must be used and the required computation time becomes prohibitive, especially for design purposes.

Another source of error in the pressure integration method is demonstrated when it is applied to the zero lift case. Specifically, it is found that the method yields a non-zero induced drag force when the test wings are analyzed at zero angle of attack. Since the wings are untwisted and the airfoil symmetric, this is clearly a numerical error and, although small, must be taken into account. Fig. 5 shows the dependence of this error on panel density for the low-order panel method used in the present study, and compares this to a similar error obtained using a higher-order method and presented in Ref. 3. The error in the zero-lift drag prediction appears to be dependent on sweep, however, increasing the number of spanwise panels causes this dependence to disappear. This behavior is corroborated by the results of Ref. 3. With 100 chordwise by 10 spanwise (100x10) panels, the error with increasing sweep is very similar to that of the hybrid method. As the panel

density is increased to 100x50, however, the error is essentially independent of the sweep. Thus, for a given number of chordwise panels, increasing the spanwise panel density causes the zero-lift error to approach that of the zero-sweep case. Consequently, a correction based on the zero-sweep error for a given chordwise density can be applied to the pressure integration drag computations. In the test cases that follow, the pressure integration results are presented both with and without the zero-lift error accounted for. These two extremes are presented as an upper and lower bound on the pressure integration results.

Finally, it should be noted that the pressure integration results presented do include an effect from the deforming wake. This comes about in the computation of the pressure on the wing surface by including the contribution of velocity induced by the deformed wake.

Trefftz Plane Method

Following the formulation by Trefftz²³, the induced drag was computed assuming the wake to be fixed and aligned with the free-stream velocity. The Trefftz method used here differs from the hybrid panel/trailing-edge method only in that the wake is undeformed. In the following comparisons, the difference in results between the hybrid method and the Trefftz method can be taken to be the influence of the freely deforming wake.

Modified Lifting Line

The last method used for comparison uses the modified lifting-line calculation of induced drag⁷. This method takes the spanwise circulation distribution predicted by the low-order panel method, computes the corresponding strength of the trailing streamwise vortex filaments shed into the wake, then relaxes the wake using only the influence of the trailing wake vortices. The induced drag is then computed applying the Kutta-Joukowski law at the wing trailing edge using the velocity induced by the deformed wake and the wing circulation assumed to be concentrated at the trailing edge. Unlike the hybrid method the modified lifting-line method does not include any influence from the wing in calculating the shape of the deformed wake.

Comparison of Results

Figs. 6 and 7 present the span efficiency factor, e , predicted by the hybrid panel/trailing-edge method, pressure integration, Trefftz method, and modified lifting-line method, as a function of the wing tip location (wing sweep). The methods all use a panelling grid with 50 chordwise (25 upper, 25 lower) and 20 spanwise (half-span) panels. Results for an angle of attack of 4 degrees are given in Fig. 6, and results for 8 degrees in Fig. 7.

The hybrid panel/trailing-edge method shows the most consistency between the 4 and 8 degree angle of attack cases; the other methods show a reversal in their predicted trends. Although it is expected that e will change slightly with angle of attack, the radical trend changes predicted by the other methods are hard to substantiate. The consistency of the hybrid method suggests that it is less prone to error at higher angles of attack than the other methods, especially pressure integration, and is therefore more robust. The reduction in induced drag with aft sweep corresponds to recent experimental results²⁴ and has been predicted by others using various methods over the past several years¹⁻³.

Drag predictions of the present method are compared with those from a higher-order panel method using pressure integration³ in Fig. 8. The higher-order panel method required 100 chordwise and 70 spanwise panels to approach a consistent result. In contrast, the hybrid panel/trailing-edge method essentially matches those results with only 50x20 panels. If it is assumed that the computation time of the panel methods vary with N^2 , the hybrid method will run approximately 50 *times faster* than the higher-order panel method for the same level of accuracy. For this reason, the hybrid panel/trailing-edge method should be an extremely useful tool for the design of wings having minimum induced drag.

VI. Validation Using Experimental Results

Description of Test Models

In addition to comparing results to a number of other methods, the hybrid panel/trailing edge method was validated by comparing its predictions against experimental results. The experimental data used are those obtained during recent wind-tunnel tests at the NASA Langley Research Center. The wing geometries used for this comparison are similar to those used in the computational validation of the previous section. Each wing has an elliptical chord distribution with spanwise varying amounts of wing sweep. The location of the quarter chord point at each spanwise station is defined by the position of the wing tip relative to the root chord and is given by the expression

$$x_{.25c} = c_r \left(\frac{x_{tip}}{c_r} \right) \left(1 - \frac{3}{4} \frac{c}{c_r} \right).$$

The wings used in the wind-tunnel tests have tip locations at 0.25 (unswept elliptical), 1.50 (crescent shaped), and 1.00 (straight trailing-edge) relative to the root chord. A constant NLF(1)-0416 airfoil section²⁵ is used on each model, and the transition point is fixed by trip strips at 7.5% chord. The wings of the wind-tunnel models are untwisted, have a span of 48.00 inches, a projected area of 384.0 sq.in., and an aspect ratio of 6.00. Each of the wings is mounted on a common 3.00 inch diameter centerbody. The influence of the centerbody is not included in the computational predictions. The geometries of these wings (without the centerbody) are shown in Fig. 9.

Prediction Method

The hybrid panel/trailing-edge method was used to predict the inviscid (vortex) induced drag. The wings were modeled with 60 chordwise (30 upper, 30 lower) panels and 20 spanwise (half-span) panels. The span efficiency factor was predicted using the same procedure as described in the previous sections.

The profile drag of the models was predicted by means of a strip analysis using the section lift coefficients predicted by the panel method. The section profile drag coefficients of the NLF(1)-0416 airfoil as a function of chord Reynolds number and section lift coefficient were obtained using the computer program developed by Eppler and Somers²⁶. The effects of flow separation at the higher lift coefficients are not fully taken into account.

Presentation and Discussion of Results

The results from the wind-tunnel tests and the predictions of the hybrid panel/trailing-edge method are presented in Figs. 10–21, and in Table 1. Comparisons between the experimentally measured and the computationally predicted performance for each wing are presented in Figs. 10–12. The drag is slightly overpredicted at low lift coefficients in all cases and underpredicted at high lift coefficients for the crescent-shaped wing. The change in drag with respect to lift is predicted fairly well up to moderate lift coefficients for all of the wings. Figs. 13 and 14 can be used to compare the performance of the wings relative to one another as measured experimentally and as predicted by the hybrid method. The predicted results agree with the measured data in that the straight-trailing-edge wing exhibits a drag lower than the unswept elliptical wing even to high lift coefficients. The prediction method does not, however, capture the significant increase in drag for the crescent-shaped wing at high lift coefficients.

The measured and the predicted drag coefficients are presented in Figs. 15–19 as a function of C_L^2 , from which Oswald's efficiency factors can be determined. The measured data in Figs. 15–17 show that all three wings have a non-constant Oswald's efficiency for the range of lift coefficients over which they were tested. In all cases the measured Oswald's efficiency decreases with increasing lift coefficient. The change is greatest for the crescent-shaped wing. As expected, the predicted Oswald's efficiencies remain fairly constant over the entire lift coefficient range. In the case of the unswept elliptical and straight-trailing-edge wings, the predicted Oswald's efficiency matches the measured efficiency over the C_L range from approximately 0.7 to 0.9. For the crescent-shaped wing, the predicted and mea-

sured Oswald's efficiencies match for lift coefficients from 0.6 to 0.8. In all cases, the hybrid method underpredicts the Oswald's efficiency at low C_L and overpredicts it at high C_L .

In Figs. 18 and 19 it can be seen that the experimental and predicted results agree in that both show the relative inferiority of the unswept elliptical wing. Based on these data and the computational results of the following sections (see Fig. 25), this result is probably due to the variance of the spanwise lift distribution from elliptical. Above a lift coefficient of 0.7, the experiment shows the crescent-shaped wing to be clearly inferior to the straight-trailing-edge wing. This is likely due to flow separation on the highly swept tips of the crescent-shaped wing. Obviously this viscous effect is not captured in the prediction method and, in fact, the predicted results actually show the straight-trailing-edge wing slightly inferior above a lift coefficient of 0.7. This discrepancy results from error in the predicted profile drag component which is added to the hybrid method's inviscid induced drag prediction. To illustrate this, the predicted *inviscid* induced drag coefficient is presented as a function of C_L^2 in Fig. 20. It can be seen that the crescent-shaped and straight-trailing-edge wings have nearly identical span efficiencies with the unswept elliptical wing being clearly inferior.

As a means of separating the effects of the viscous and the inviscid drag components at lift coefficients between 0 and 0.7, Fig. 21 presents a comparison between the measured (total) drag coefficient and the predicted vortex (inviscid) induced drag coefficient both as functions of C_L^2 . The predicted curves have been offset by a constant amount to aid in comparing their slopes to those of the measured data. It can be seen in this figure that for the unswept elliptical wing the measured Oswald's efficiency matches the predicted span efficiency over this entire range of lift coefficients. For the other two wings, the drag due to lift analysis must be separated into moderate and low lift coefficient ranges. In the moderate C_L range (0.4 to 0.7) the measured drag due to lift of the crescent-shaped wing becomes dominated by the drag increase due to flow separation at the tips. This is illustrated in Fig. 21 by the departure of the measured drag from the linear C_D vs. C_L^2 relationship above a lift

coefficient of 0.5. In the low C_L range (0 to 0.4) the measured data of the straight-trailing-edge wing has the most pronounced departure from the linear C_D vs. C_L^2 relationship. It is believed that this wing takes advantage of the decreasing section profile drag of the airfoil as lift is increased from $C_L = 0$ to $C_L = 0.4$ without experiencing the detrimental effects of wake roll-up as experienced by the unswept elliptical wing, or the tip flow separation experienced by the crescent-shaped wing. The straight-trailing-edge wing actually attains a measured Oswald's efficiency greater than unity in the lift coefficient range between 0 and 0.7. The measured and predicted Oswald's efficiencies over the C_L range of 0 to 0.7, and the predicted span efficiency over the entire C_L range are presented in Table 1.

VII. Discussion of Design Tools for Planar and Non-Planar Wings Having Minimum Induced Drag

In order to design wings having minimum induced drag, it is necessary to know the optimum lift distribution in the presence of the freely deforming wake. Using the lifting-line model, Munk⁵ concluded that for the induced drag of a wing to be a minimum, the induced downwash at the lifting line must be constant if the wing is planar, or given by the relation

$$w_i = w_o \cos \theta$$

where w_o is a constant and θ the local dihedral angle, if the wing is non-planar. Although Munk assumed that the wake was non-deforming, the reasoning leading to the above conclusion is not dependent upon the mechanism which generates the downwash. In other words, this conclusion is valid whether the wake is fixed, or free to deform. In determining the spanwise lift distribution which generates the optimum downwash distribution, the assumption of the fixed wake does become important. The classical result of the optimum elliptic lift distribution follows immediately if this assumption is made. The question that remains, however, is what lift distribution generates the optimum downwash distribution for minimum induced drag in the presence of a free wake. As there is no mathematical solution to this question available, a first step in addressing it was taken when, in the course of this research, it was shown that for a straight lifting line with an elliptic lift distribution the induced drag is independent of wake rollup. Given this result and in lieu of a complete mathematical proof, it is assumed that the free wake does not significantly alter Munk's result concerning the optimal lift distribution for the minimization of induced drag. To test this assumption the induced drag was calculated using the modified lifting-line method with an optimal lift distribution prescribed according to Munk's result. The induced drag was then calculated with the lift distribution slightly perturbed from the prescribed optimum. In all cases considered, the drag increased. Thus, for the present time, even if the Munk result is not truly optimal, it is considered to be close enough for engineering purposes.

The effect of the deforming wake on the spanwise lift distribution of three wings with elliptic chord distributions can be seen in Figs. 22–24 which present the *error* in the spanwise lift distribution from the optimum. It can be seen that the deforming wake has the largest effect on the wing with the tip at 0.25 root chord (straight quarter-chord line). As the tip is swept aft, the wake deformation has less and less effect on the lift distribution. This is demonstrated in Fig. 23 for the straight-trailing-edge wing and in Fig. 24 for the crescent-shaped wing. It is suggested that the aft-swept tip isolates the rolled wake from the rest of the wing and, consequently, decreases its influence. These results are combined and presented in Fig. 25 where it can be seen that the straight-trailing-edge wing maintains the closest to optimal lift distribution, particularly near to the tip. This is probably due to the moderate tip sweep decreasing the effect of the rolled wake while not exacerbating the three-dimensional tip flow exhibited by the highly swept tips of the crescent-shaped wing. It is interesting to note, that even though the lift distribution of the crescent-shaped wing is farther from elliptical than the straight-trailing-edge wing, the results presented in the previous sections predict the crescent-shaped wing to have slightly higher span efficiency. Some part of this effect is likely due to the benefit of moving the wake aft more than offsets the penalty of the lift distribution not being elliptical. A more significant contribution to this effect, however, is that because the panel method predicts negative lift at the tip, application of the Kutta-Joukowski law here results in a small amount of “induced thrust,” overcoming the deficiency of the non-optimum lift distribution. This effect is very small and certainly nullified by viscous effects in the real flow. This conclusion is supported by the previously presented experimental results.

The use of the hybrid panel/trailing-edge method for the design of non-planar wings for minimum induced drag, is illustrated in Fig. 26. At the top of this figure, the lift distribution error from optimum is plotted against span for an arbitrary (starting) wing planform geometry. In this case, the wing under consideration has winglets which are 0.1 semi-span in height. Based on the error, the chord was adjusted appropriately in the

locations where it is over or under that needed for the optimum lift distribution. As shown in the other two graphs, the lift distributions for the second and third geometry iterations are closer to optimum. While these iterations are presented only to demonstrate the potential, it is clear that this process can be continued until convergence to the optimum span lift distribution is achieved. The same optimization procedure can be applied to any non-planar geometries with different dihedral distributions or winglet configurations and their overall performances compared. In this way, the hybrid method provides a valuable tool for the design of a mission specific, optimum non-planar wings.

VIII. Conclusions and Recommendations

The newly developed hybrid panel/trailing-edge method is a valuable tool for taking the non-linear effects of a freely deforming wake into account in determining the induced drag of planar and non-planar wing geometries. When compared to other methods, it is found that it achieves equivalent accuracy in considerably less computation time. Given its speed and robustness, the hybrid method should prove most useful in the design of planar and non-planar wings having minimum induced drag.

Using the hybrid panel/trailing-edge method, the influence of planform geometry on the induced drag of planar wings has been explored. It is found that the benefit of crescent-shaped planforms for reducing induced drag that has been noted by others is confirmed; however, this benefit is not nearly as great as has sometimes been suggested. For the family of wings considered, the reduction in induced drag that is possible for a wing operating at a lift coefficient of 1.0 and having a straight trailing edge as compared to one having no sweep is approximately 1%. For any additional sweep, the additional reduction in induced drag is not significant and certainly not enough to offset the penalties due to viscous effects that accompany the highly swept crescent planforms.

In exploring the effect of the freely deforming wake on the wing lift distribution, it is found that the free wake has a significant influence on the lift distribution of the unswept elliptical wing, but this effect is diminished when the tip is swept aft. Once the tip is moved back such that the wing has a straight trailing edge, any further sweep seems to have little effect on the lift distribution and, consequently, the span efficiency.

While the impact of planform shape on reducing the induced drag of planar wings is limited, significantly greater gains appear to be possible using non-planar wing configurations. While well-suited non-planar wing design methods have not been available, the speed and accuracy of the hybrid method make it ideal for this problem. Based on the few non-planar cases examined thus far, the method appears to handle these cases as well

as it does planar ones. By combining the hybrid method for analyzing induced drag with methods that predict profile drag, wing geometries which have minimum overall drag can be designed.

At this point, it is recommended that the methods developed be used to design a wind-tunnel experiment to compare mission specific planar and non-planar wings. As there is no common basis of comparison otherwise, by designing an optimum planar and an optimum non-planar wing to the same mission requirements it is possible to determine if the gains promised by non-planar geometries are, or are not, real. In addition, as quality experimental data for non-planar wings is non-existent, the results of such an experiment would be invaluable for the development and calibration of any non-planar wing analysis methods.

Finally, if the results of the recommended experiment support the promise that aerodynamic gains are possible using non-planar wing geometries, then it remains to develop a method that includes the effects of compressibility and allows a designer to trade-off these gains against other factors such as weight, wing-root bending moment, and so forth.

IX. References

1. Van Dam, C.P., "Induced-Drag Characteristics of Crescent-Moon-Shaped Wings," *Journal of Aircraft*, Vol. 24, No. 2, February 1987, pp. 115-119.
2. Kroo, I., and Smith, S.C., "The Computation of Induced Drag with Nonplanar and Deformed Wakes," SAE 901933, SAE Aerospace Technology Conference and Exposition, October 1990.
3. DeHaan, M.A., "Induced Drag of Wings With Highly Swept and Tapered Wing Tips," AIAA-90-3062-CP, *AIAA 8th Applied Aerodynamics Conference, A Collection of Technical Papers*, August 1990, pp. 571-581.
4. Prandtl, L., "Applications of Modern Hydrodynamics to Aeronautics," NACA Report No. 116, 1921.
5. Munk, M.M., "The Minimum Induced Drag of Aerofoils," NACA Report No. 121, 1921.
6. Cone, C.D., Jr., "The Theory of Induced Lift and Minimum Induced Drag of Nonplanar Lifting Systems," NASA TR R-139, 1962.
7. Eppler, R., "Die Entwicklung der Tragflügeltheorie," *Z. Flugwiss*, November 1987, pp. 133-144.
8. Falkner, V.M., "The Calculation of Aerodynamic Loading on Surfaces of Any Shape," ARC R&M 1910, 1943.
9. Butter, D.J., and Hancock, G.J., "A Numerical Method for Calculating the Trailing Vortex System behind a Swept Wing at Low Speed," *The Aeronautical Journal of the Royal Aeronautical Society*, Vol. 75, August 1971, pp 564-568.
10. Schlichting, H. and Thomas, H.H.B.M., "Note on the Calculation of the Lift Distribution of Swept Wings," R.A.E. Report No. AERO 2236, December 1947.
11. Robinson, A. and Laurmann, M.A., *Wing Theory*, Cambridge University Press, Cambridge, 1956.
12. Schlichting, H. and Truckenbrodt, E., *Aerodynamics of the Airplane*, McGraw-Hill, New York, 1979.
13. Jones, R.T. and Cohen, D., *High-Speed Wing Theory*, Princeton University Press, Princeton, 1960.
14. Katz, J. and Plotkin, A., *Low-Speed Aerodynamics*, McGraw-Hill, New York, 1991.
15. Maskew, B., "Prediction of Subsonic Aerodynamic Characteristics: A Case for Low-Order Panel Methods," *Journal of Aircraft*, Vol. 19, Feb. 1982, pp. 157-163.

16. Samant, S.S., Bussoletti, J.E., Johnson, F.T., Burkhart, R.H., Everson, B.L., Melvin, R.G., and Young, D.P., "TRANAIR: A Computer Code for Transonic Analysis of Arbitrary Configurations," AIAA Paper 87-0034, January 1987.
17. Van Dam, C.P., Nikfetrat, K., Vijgen, P.M.H.W., and Fremaux, C.M., "Calculation and Measurement of Induced Drag at Low Speeds," SAE 901935, SAE Aerospace Technology Conference and Exposition, October 1990.
18. Tinocco, E.N., "CFD Applications to Complex Configurations: A Survey," *Applied Computational Aerodynamics*, Henne, P.A. (ed.), *AIAA Progress in Aeronautics and Astronautics*, Washington, D.C., Vol. 125, Chapter 15, pp. 559-615.
19. Konstadinopoulos, P., Thrasher, D.F., Mook, D.T., Nayfeh, A.H., and Watson, L., "A Vortex-Lattice for General Unsteady Aerodynamics," *Journal of Aircraft*, Vol. 22, 1985, pp. 43-49.
20. Ashby, D.L., Dudley, M., Iguchi, S.K., "Development and Validation of an Advanced Low-Order Panel Method," NASA TM 101024, 1988.
21. Rossow, V.J., "Theoretical Study of Lift-Generated Vortex Wakes Designed to Avoid Rollup," *AIAA Journal*, Vol. 13, No. 4, 1975, pp 476-484.
22. Higdon, J.J.L., and Pozrikidis, E., "The Self-Induced Motion of Vortex Sheets," *Journal of Fluid Mechanics*, Vol. 150, 1985, pp. 203-231.
23. Trefftz, E., "Prandtl'sche Tragflächen und Propellertheorie," *Z. angew. Math. Mech.*, Vol. 1, 1921, p. 206
24. Van Dam, C.P., Nikfetrat, K., Chang, I.C., and Vijgen, P.M.H.W., "Drag Calculations of Wings Using Euler Methods," AIAA-91-0338, AIAA 29th Aerospace Sciences Meeting, 1991.
25. Somers, D.M., "Design and Experimental Results for a Natural-Laminar-Flow Airfoil for General Aviation Applications," NASA TP 1861, 1981.
26. Eppler, R. and Somers, D.M., "A Computer Program for the Design and Analysis of Low-Speed Airfoils," NASA TM 80210, 1980.

Wing Geometry	Oswald's Efficiency Factor $0 < C_L < 0.7$		Span Efficiency Factor
	Measured	Predicted	
Unswapt Elliptical	.9691	.9248	.9754
Crescent Shaped	.9800	.9463	.9866
Straight Trailing Edge	1.0102	.9381	.9823

Table 1: Measured and Predicted Efficiency Factors for the NASA LaRC Test Wings

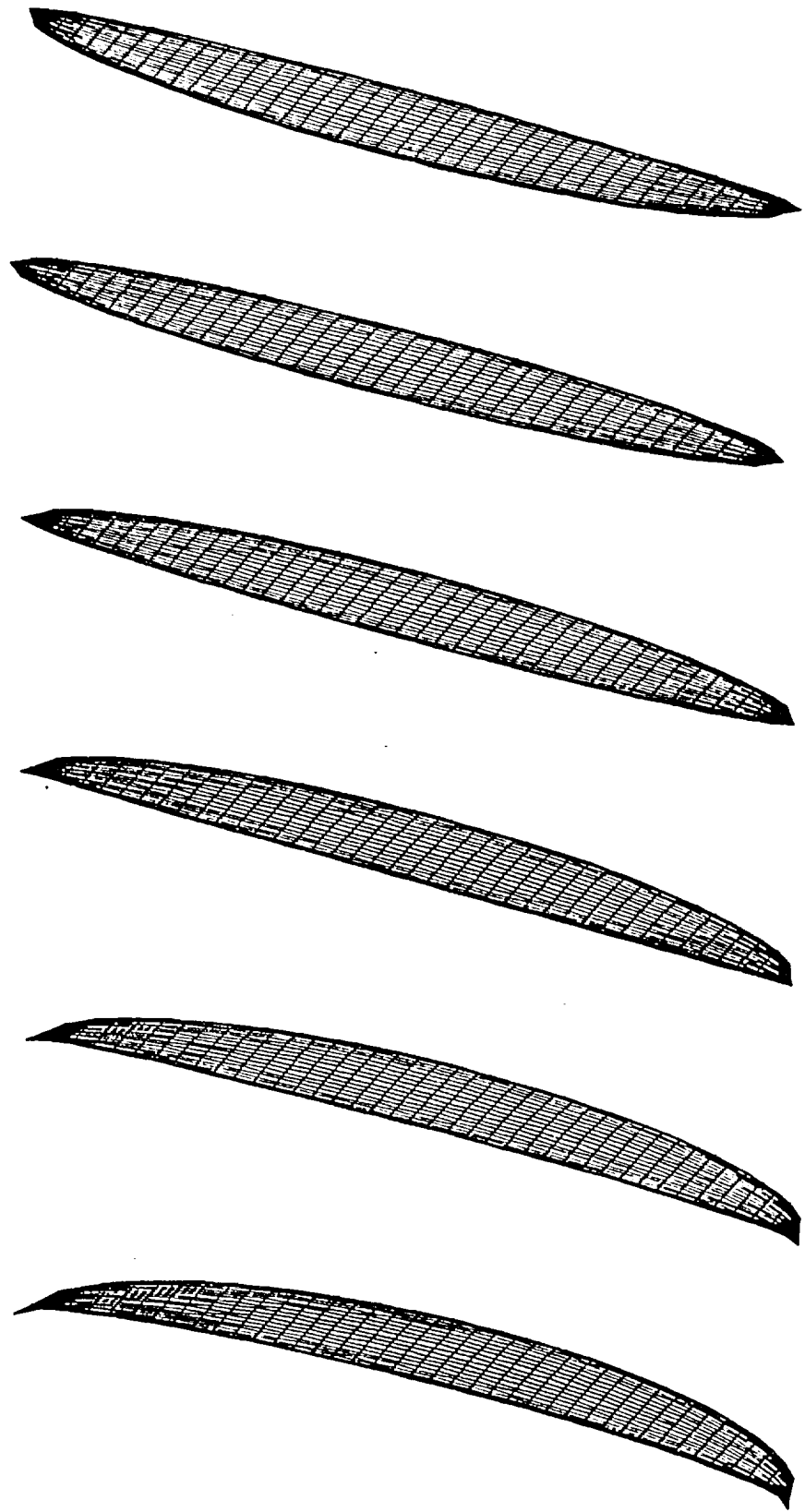


Figure 1: Wing Geometries Used for the Computational Validation of the Hybrid Panel/Trailing-Edge Method from Unswept Elliptical Wing (top) to Full Crescent-Shaped Wing (bottom).

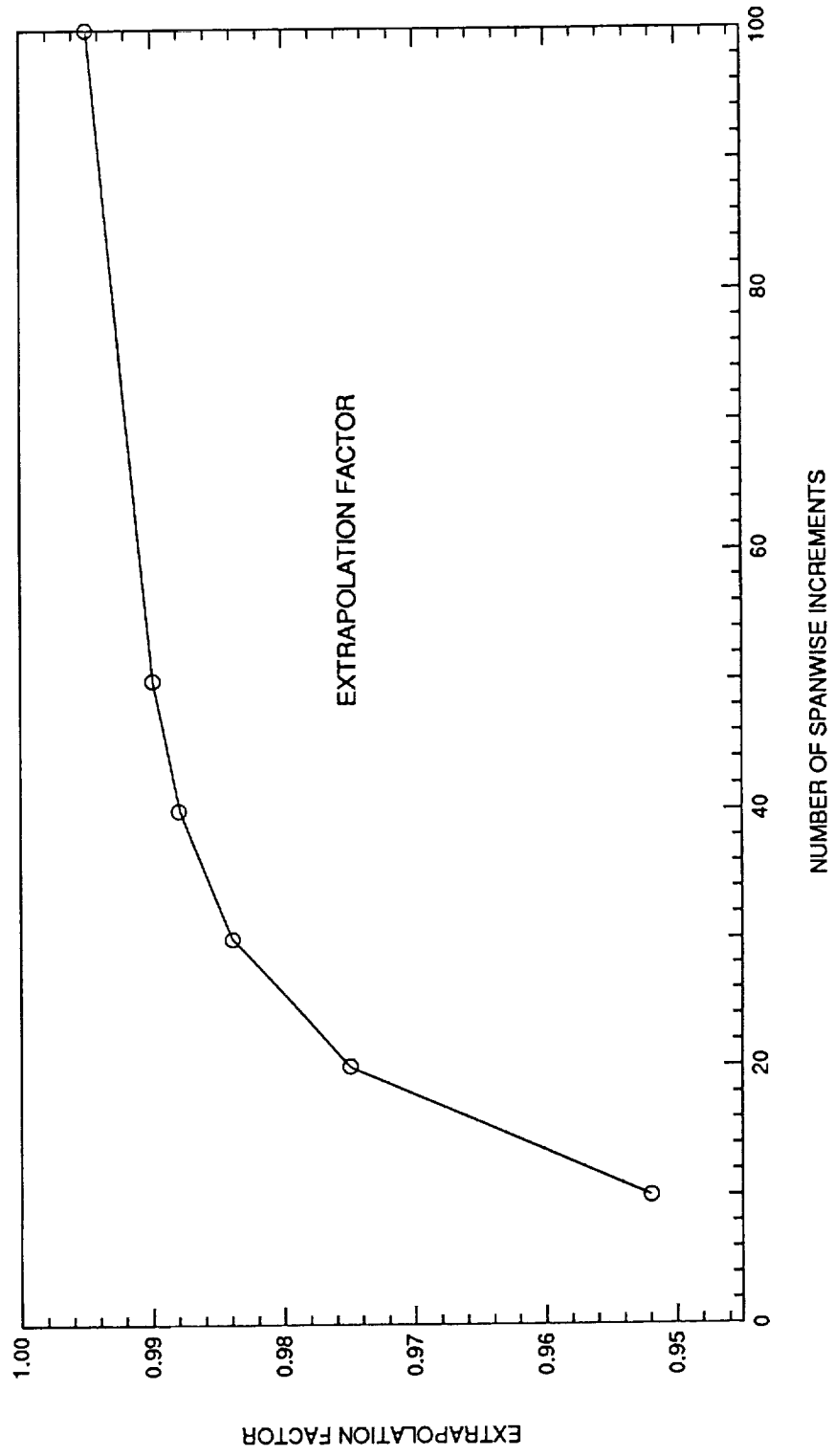


Figure 2: Extrapolation Factor for Hybrid Panel/Trailing-Edge Method

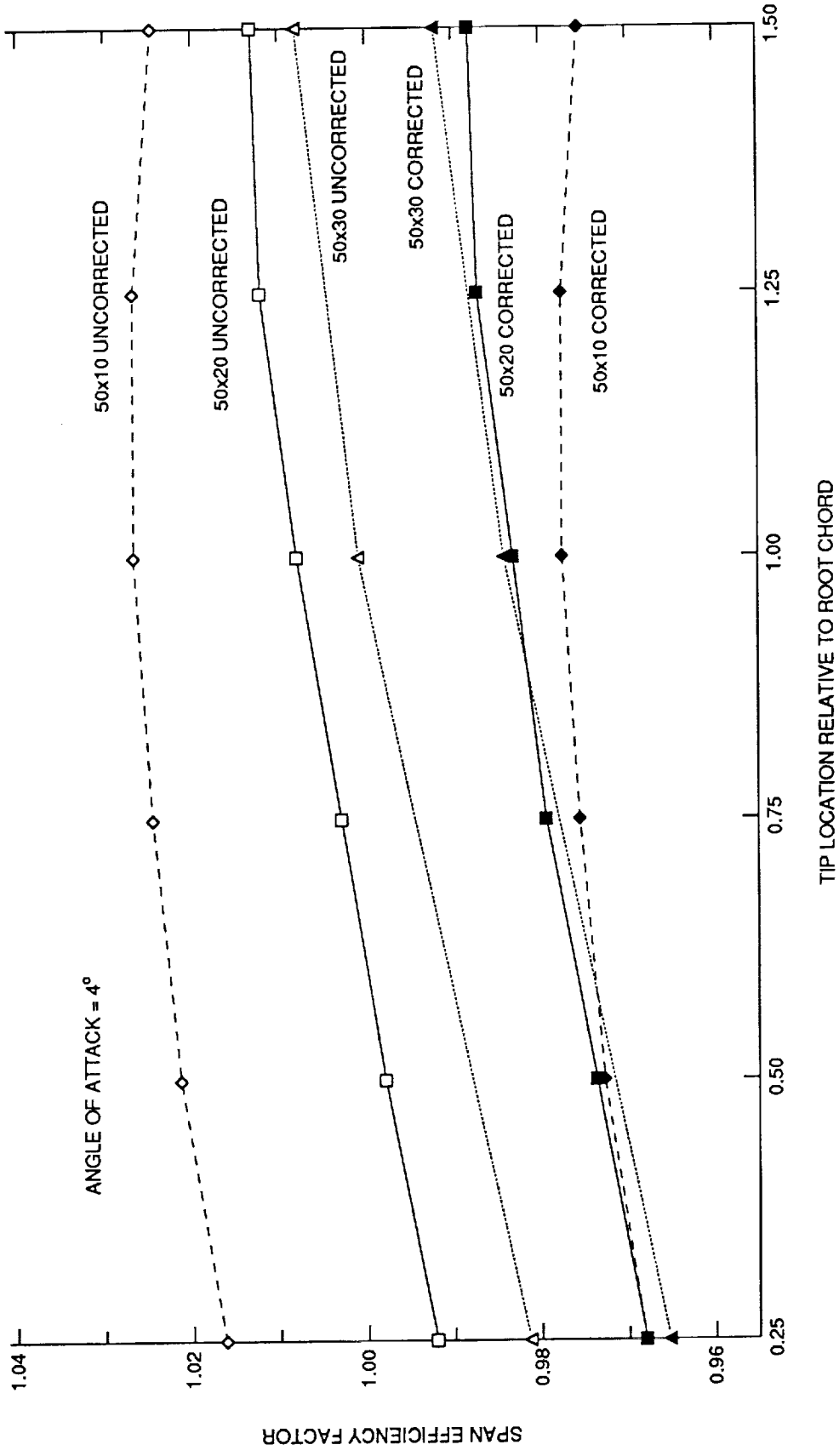


Figure 3: Effect of Extrapolation Factor Correction on Results from the Hybrid Panel/Trailing-Edge Method, 4 degrees Angle of Attack

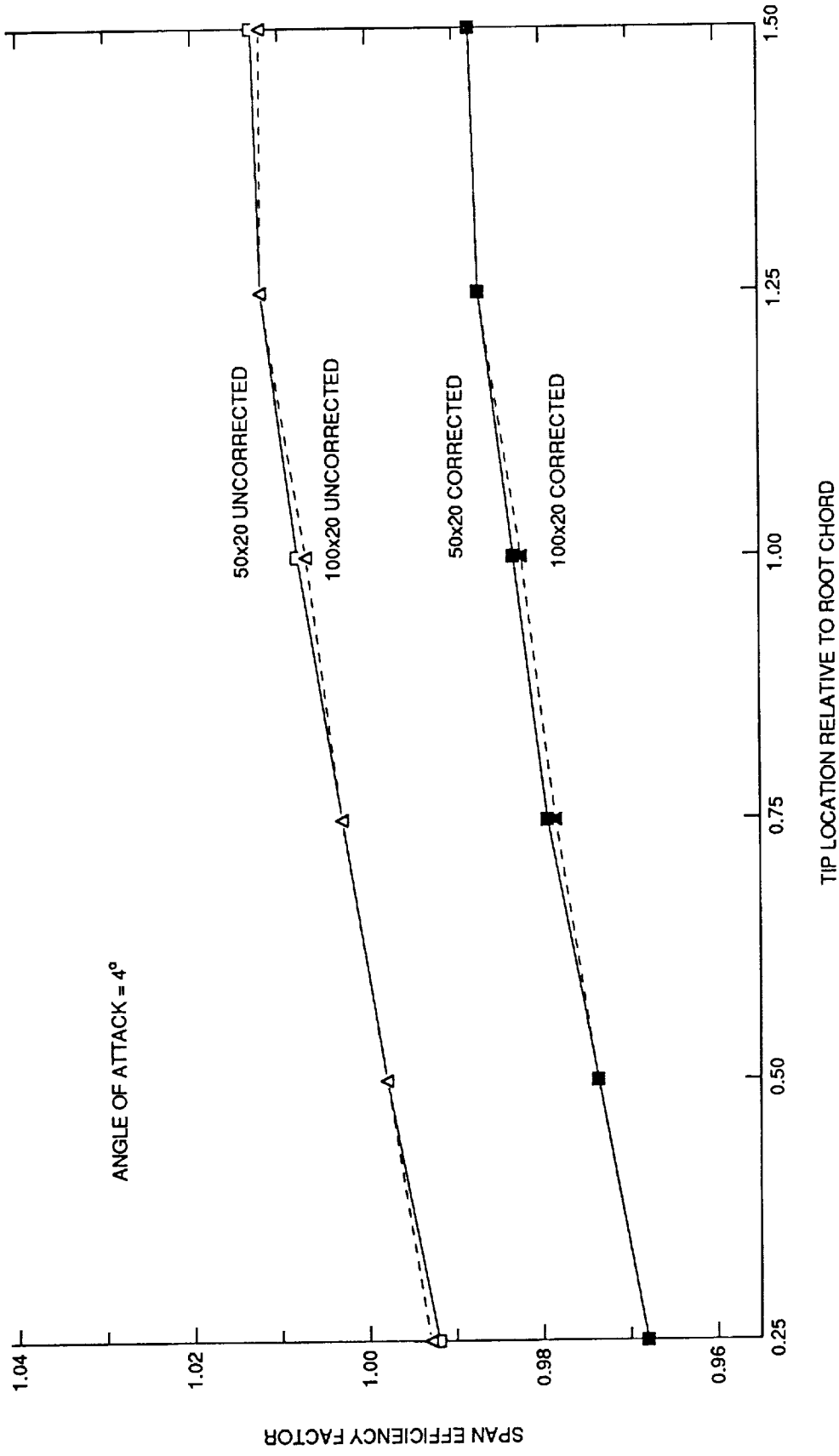


Figure 4: Dependence of Span Efficiency Factor on Chordwise Panel Spacing, 4 degrees Angle of Attack

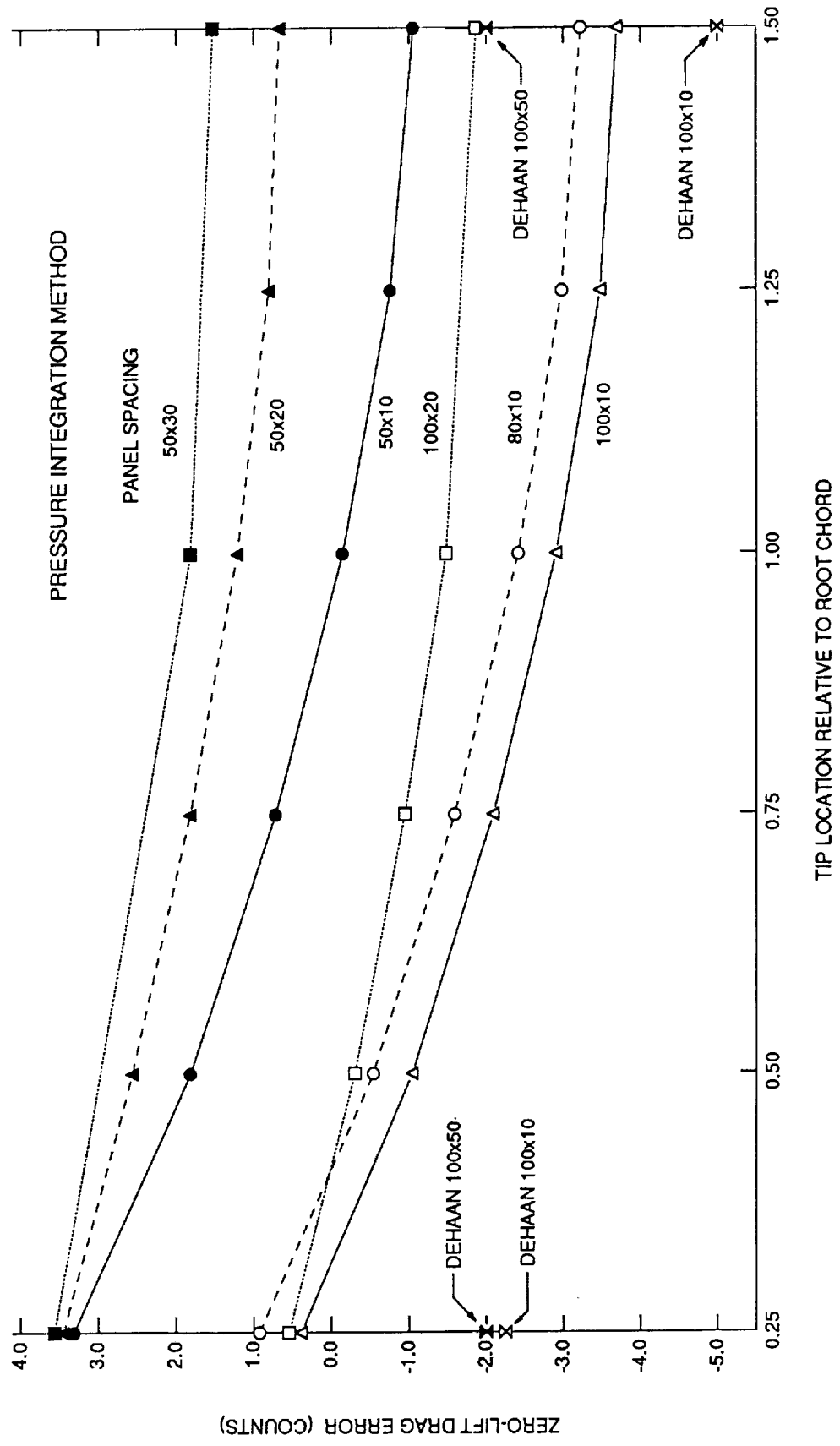


Figure 5: Pressure Integration Method Zero-Lift Drag Error

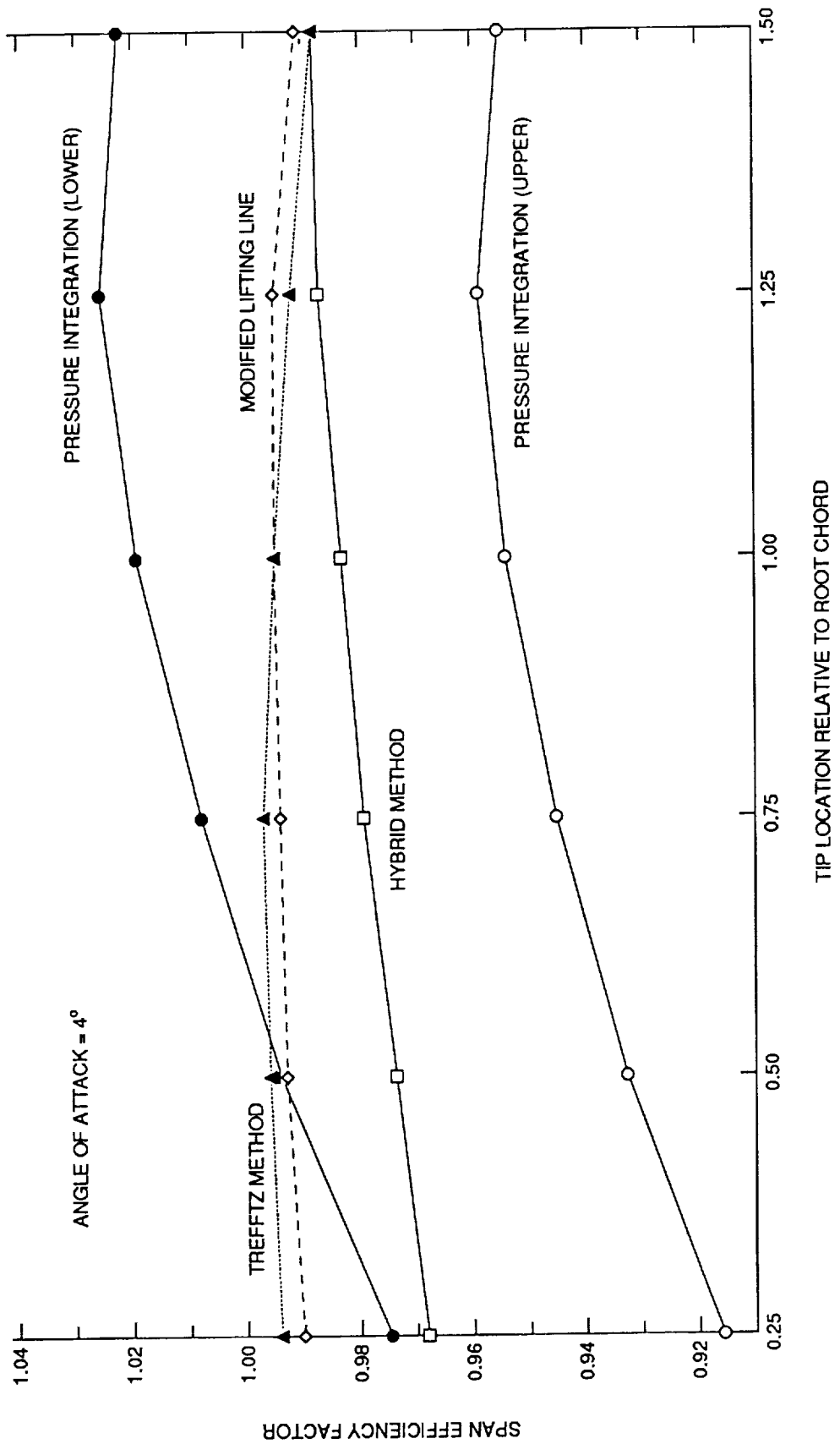


Figure 6: Comparison of Induced Drag Prediction Methods, 4 degrees Angle of Attack

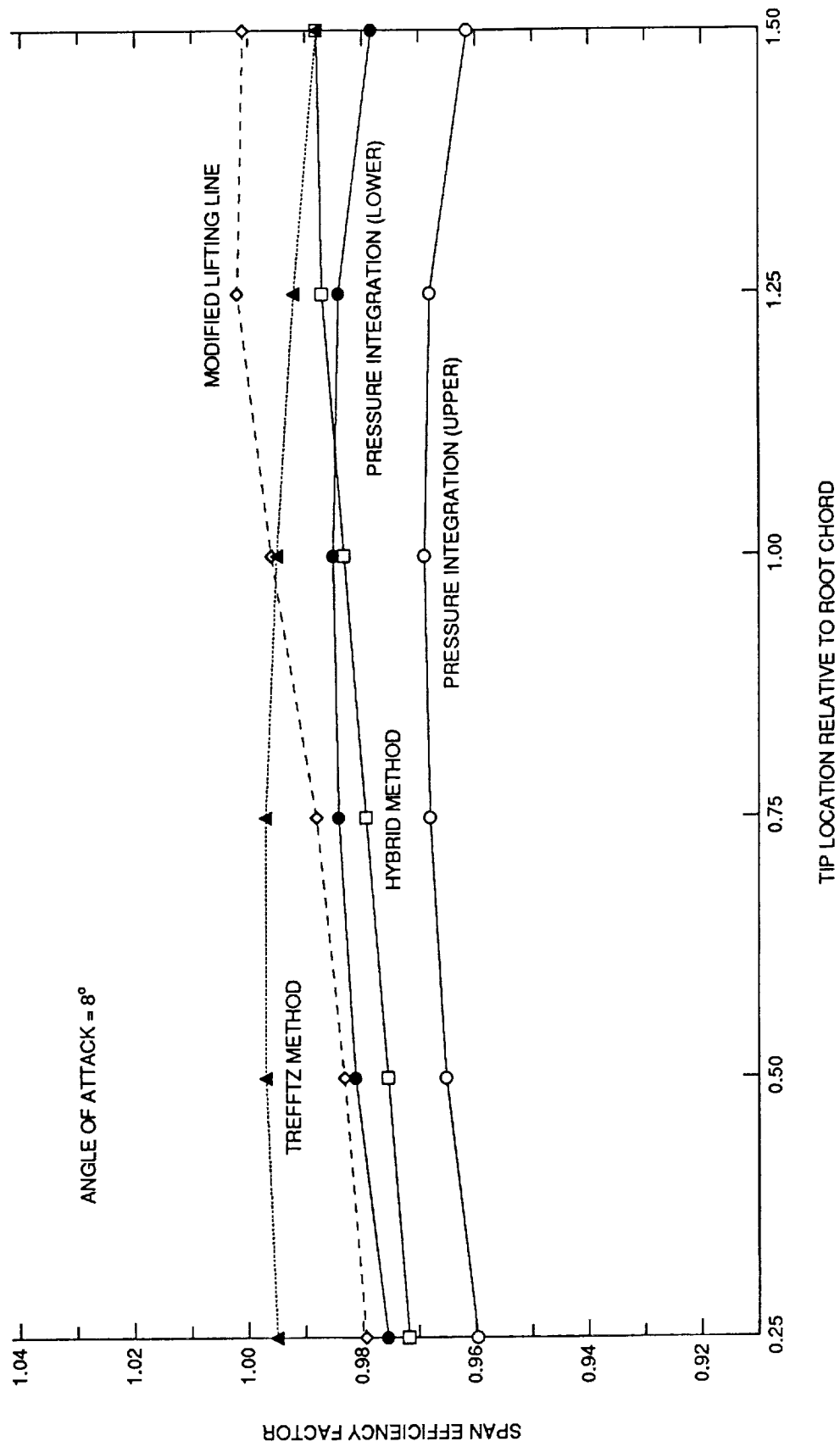


Figure 7: Comparison of Induced Drag Prediction Methods, 8 degrees Angle of Attack

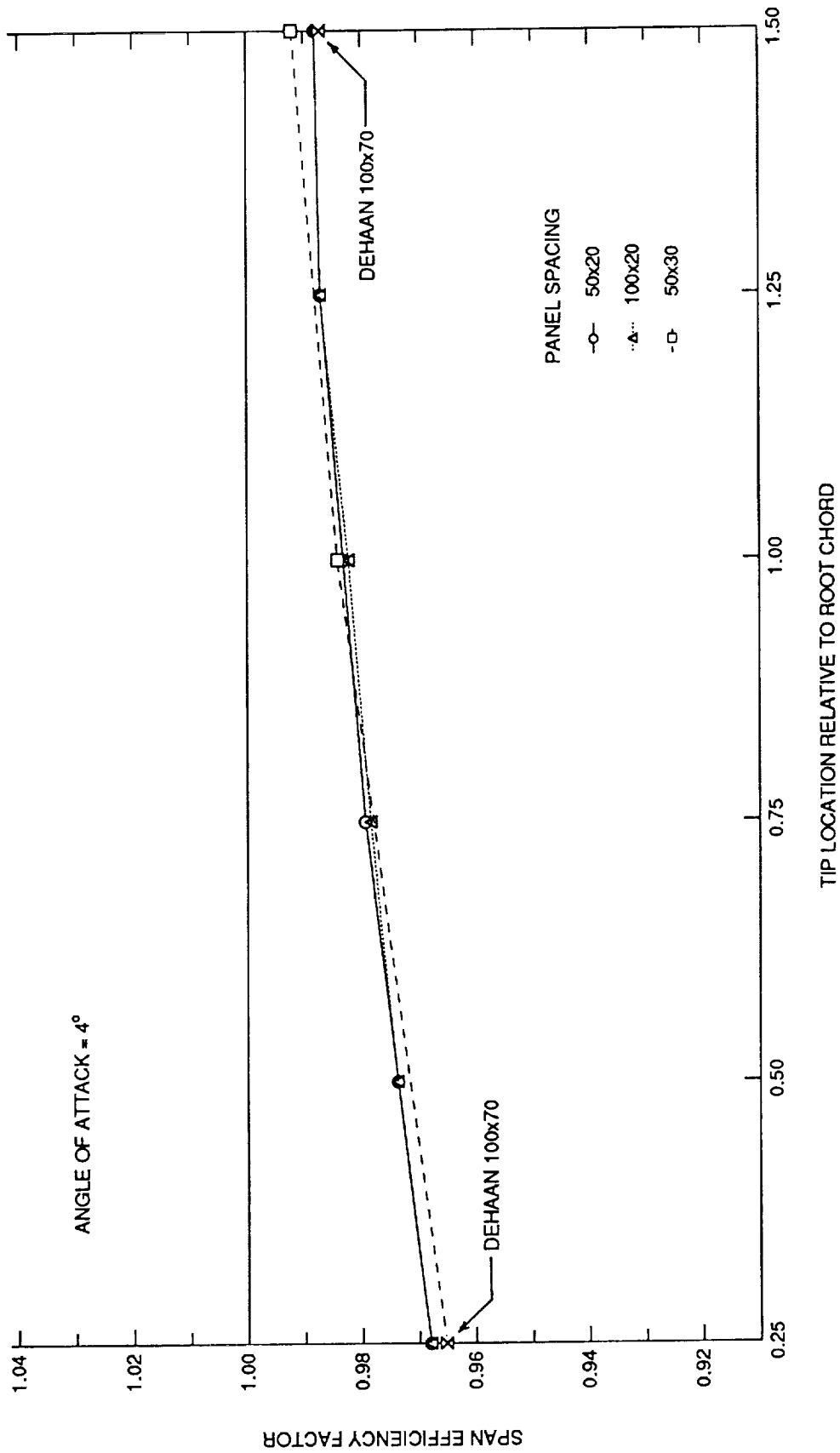


Figure 8: Comparison of Results between the Hybrid Panel/Trailing-Edge Method and a Higher-Order Panel Method

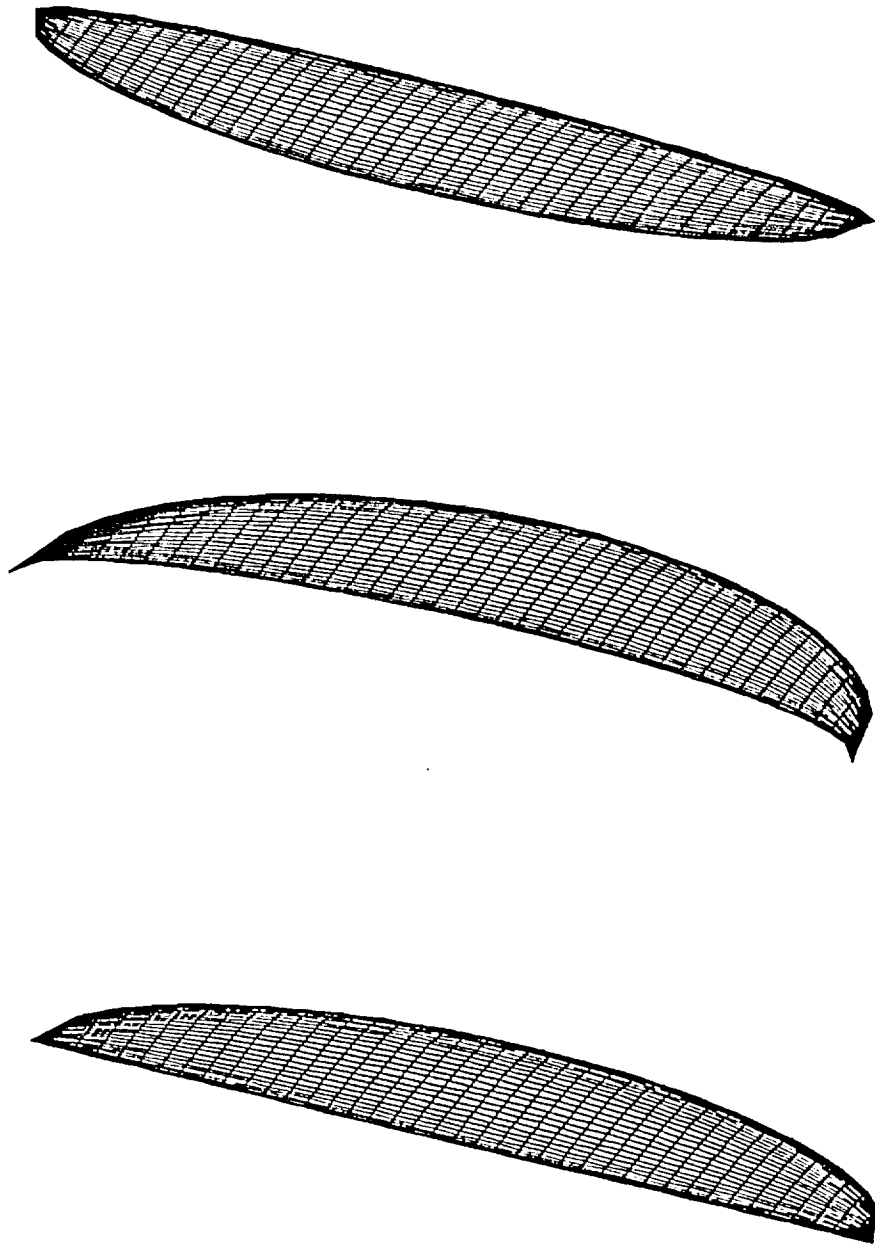


Figure 9: Wing Geometries Used for the Experimental Validation of the Hybrid Panel/Trailing-Edge Method; Unswept Elliptical (top), Crescent-Shaped (center), and Straight Trailing-Edge (bottom)

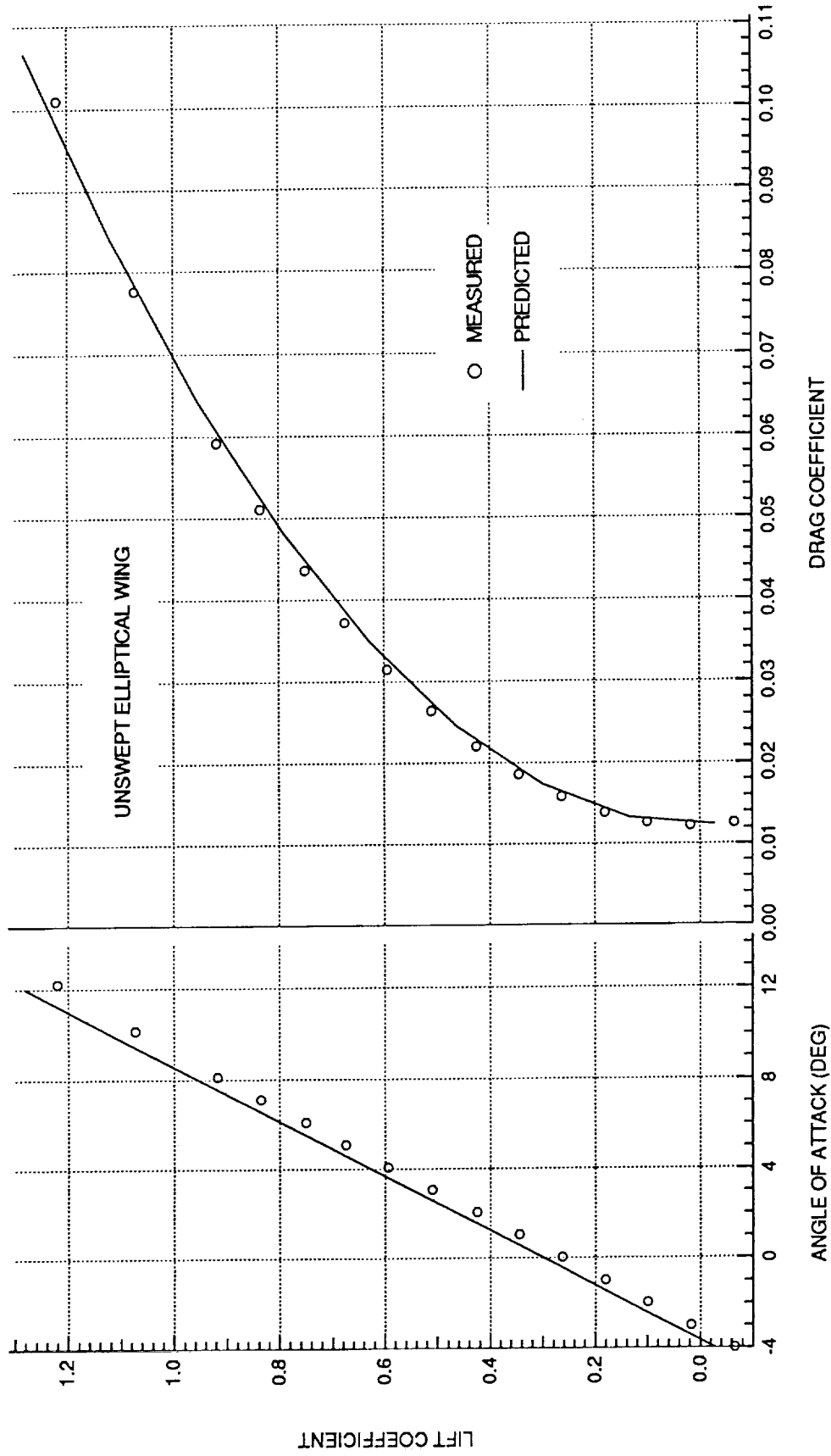


Figure 10: Comparison of the Measured and Predicted Lift and Drag of the Unswept Elliptical Wing

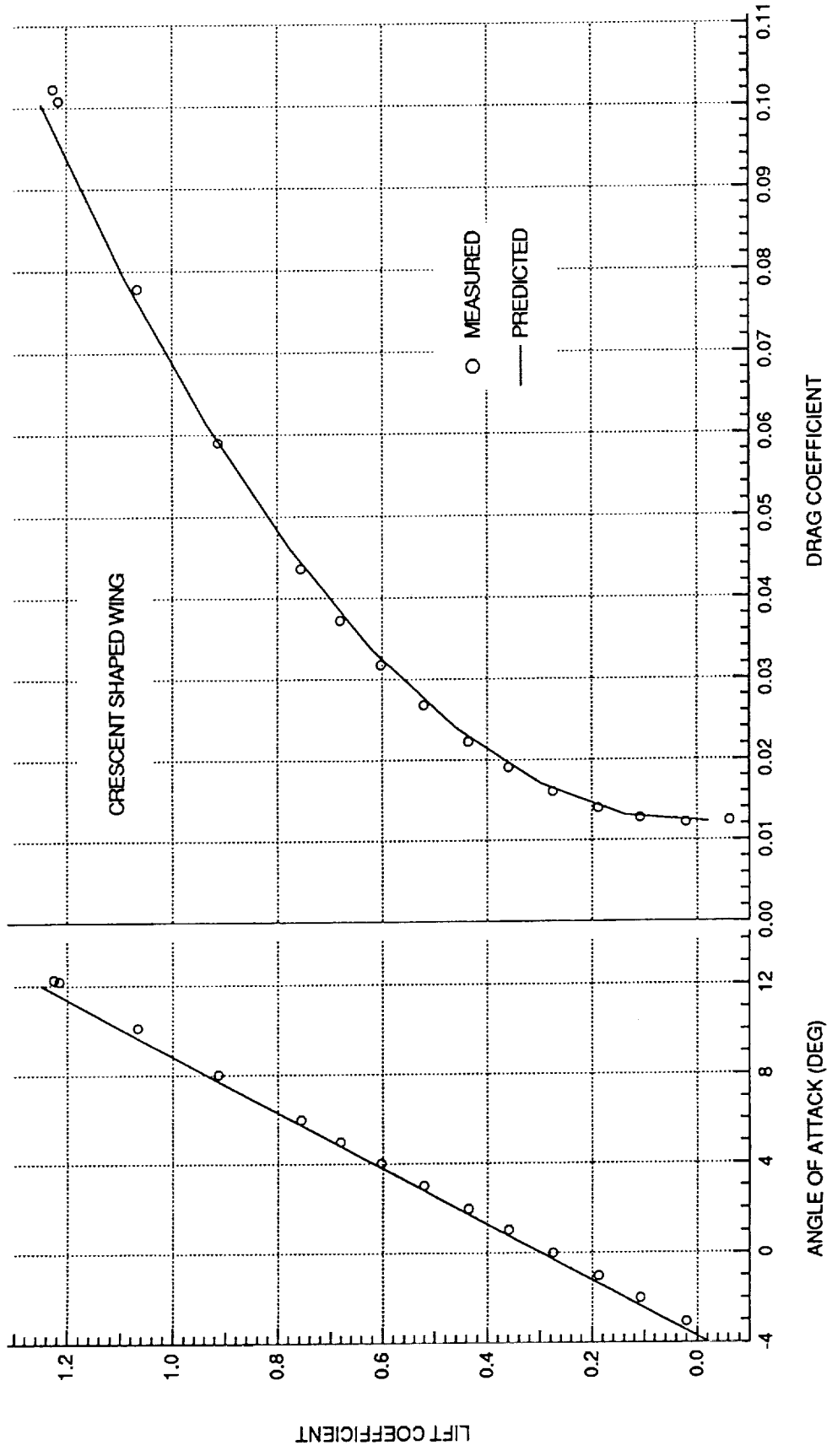


Figure 11: Comparison of the Measured and Predicted Lift and Drag of the Crescent Shaped Wing

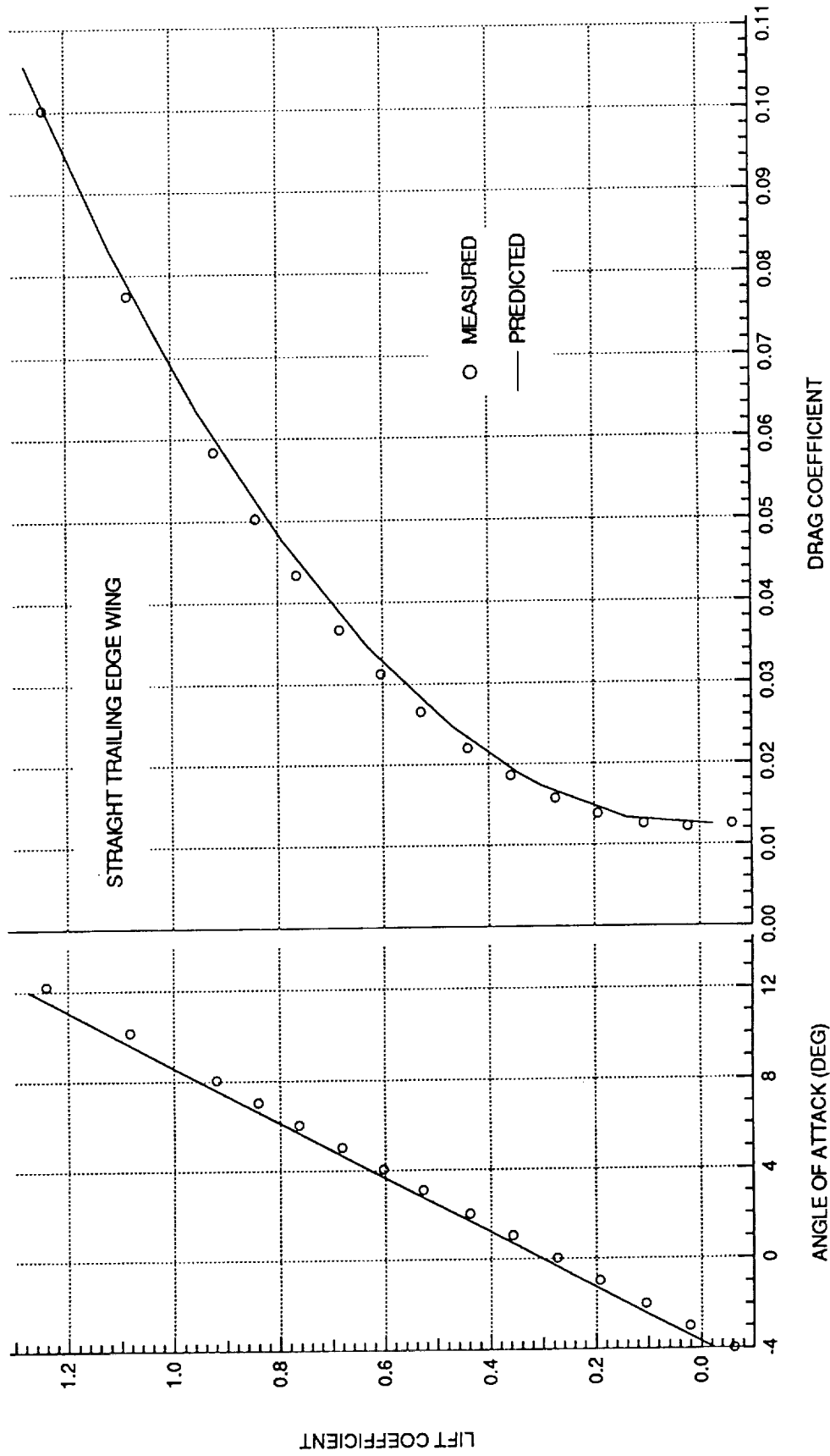


Figure 12: Comparison of the Measured and Predicted Lift and Drag of the Straight Trailing Edge Wing

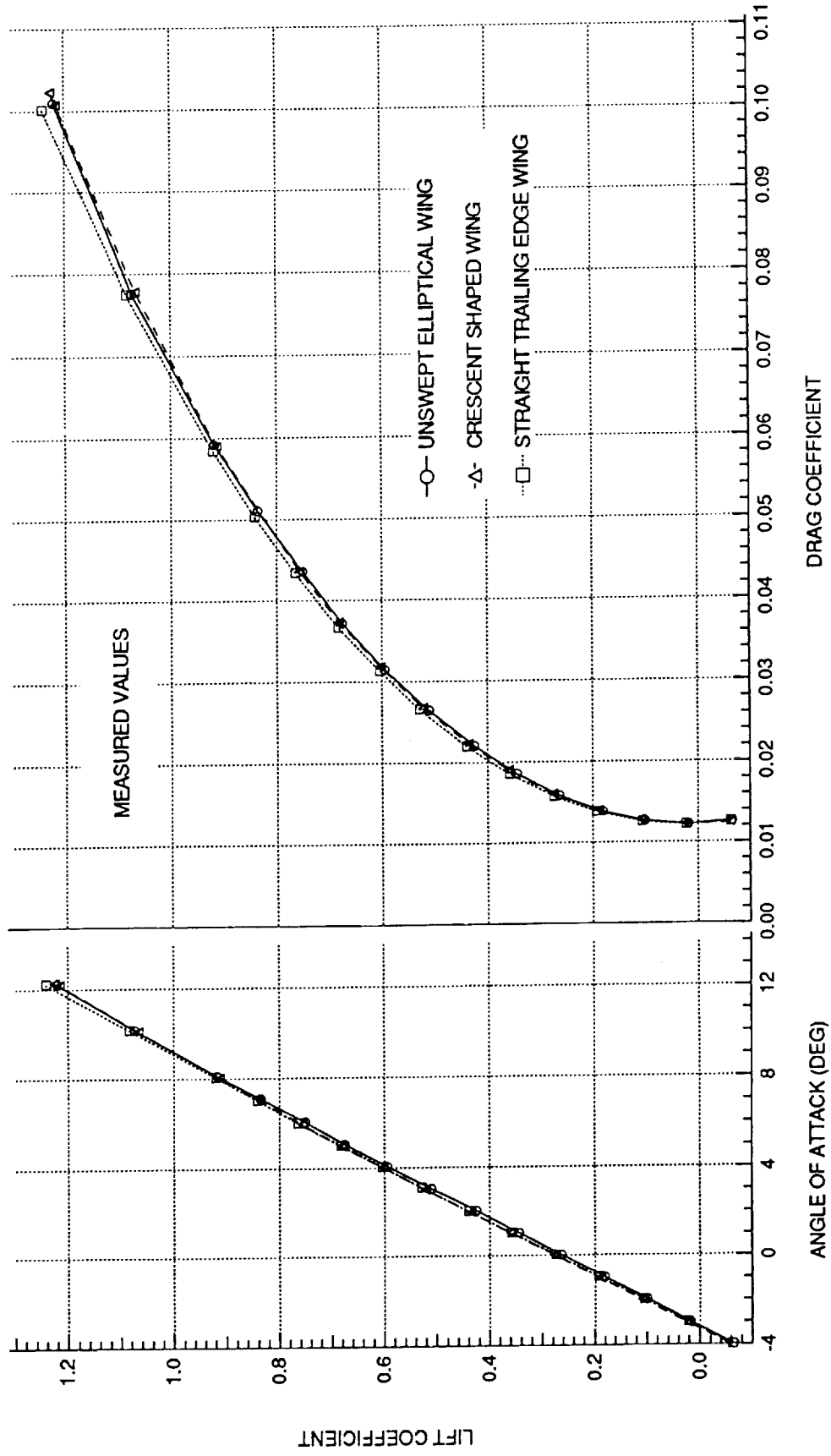


Figure 13: Comparison of the Measured Lift and Drag of the NASA LaRC Test Wings

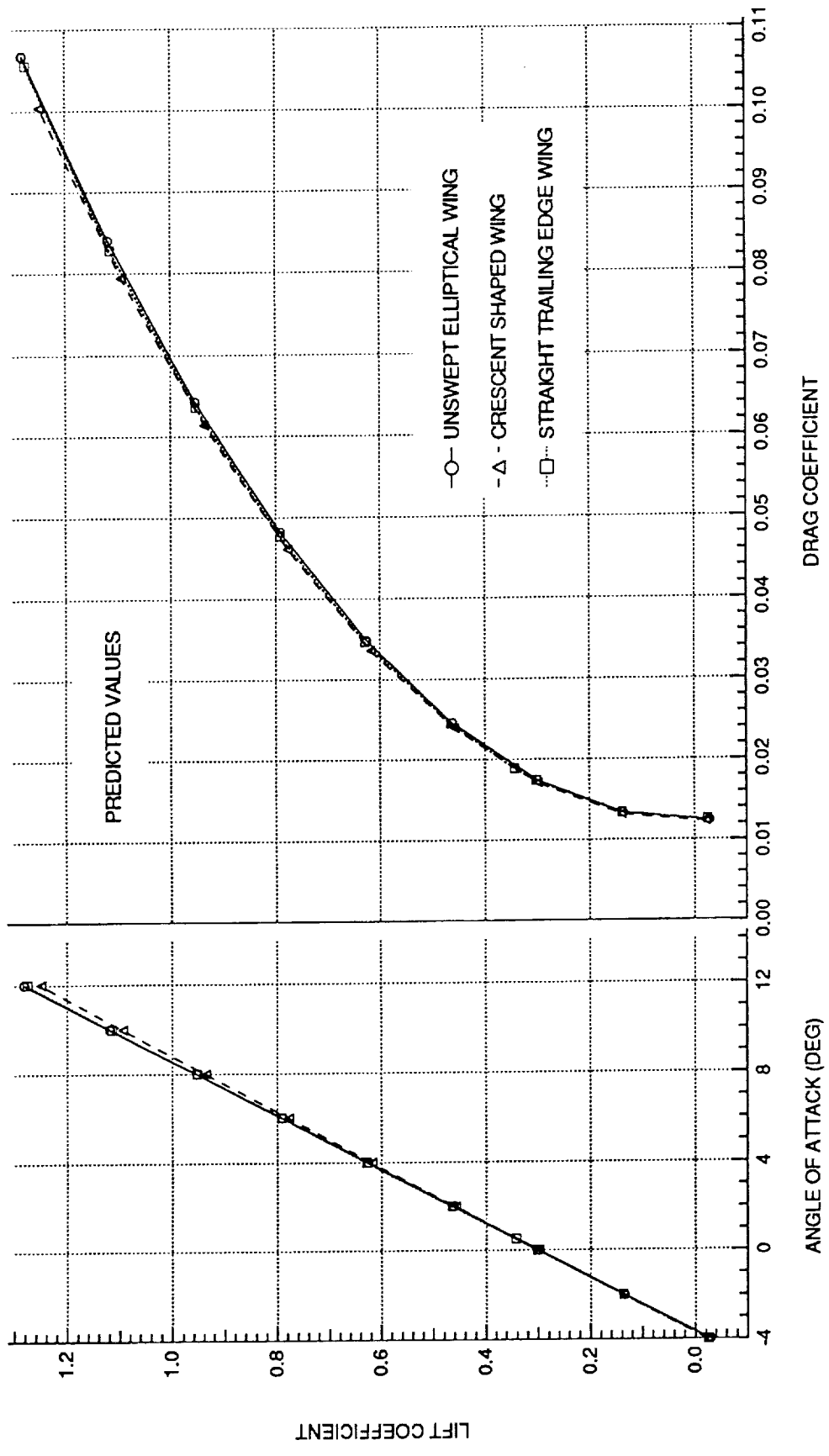


Figure 14: Comparison of the Predicted Lift and Drag of the NASA LaRC Test Wings

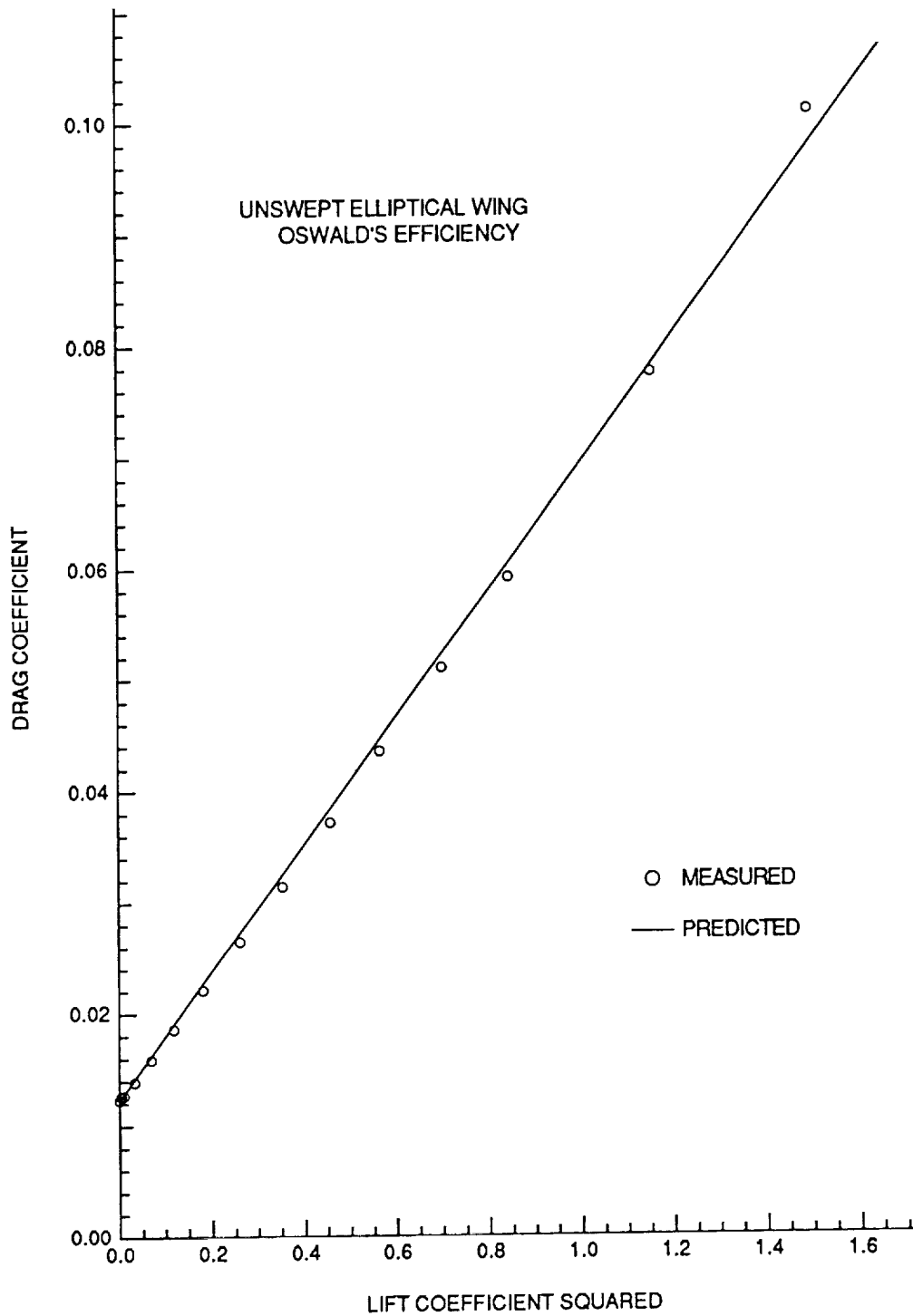


Figure 15: Comparison of the Measured and Predicted Oswald's Efficiencies for the Unswept Elliptical Wing

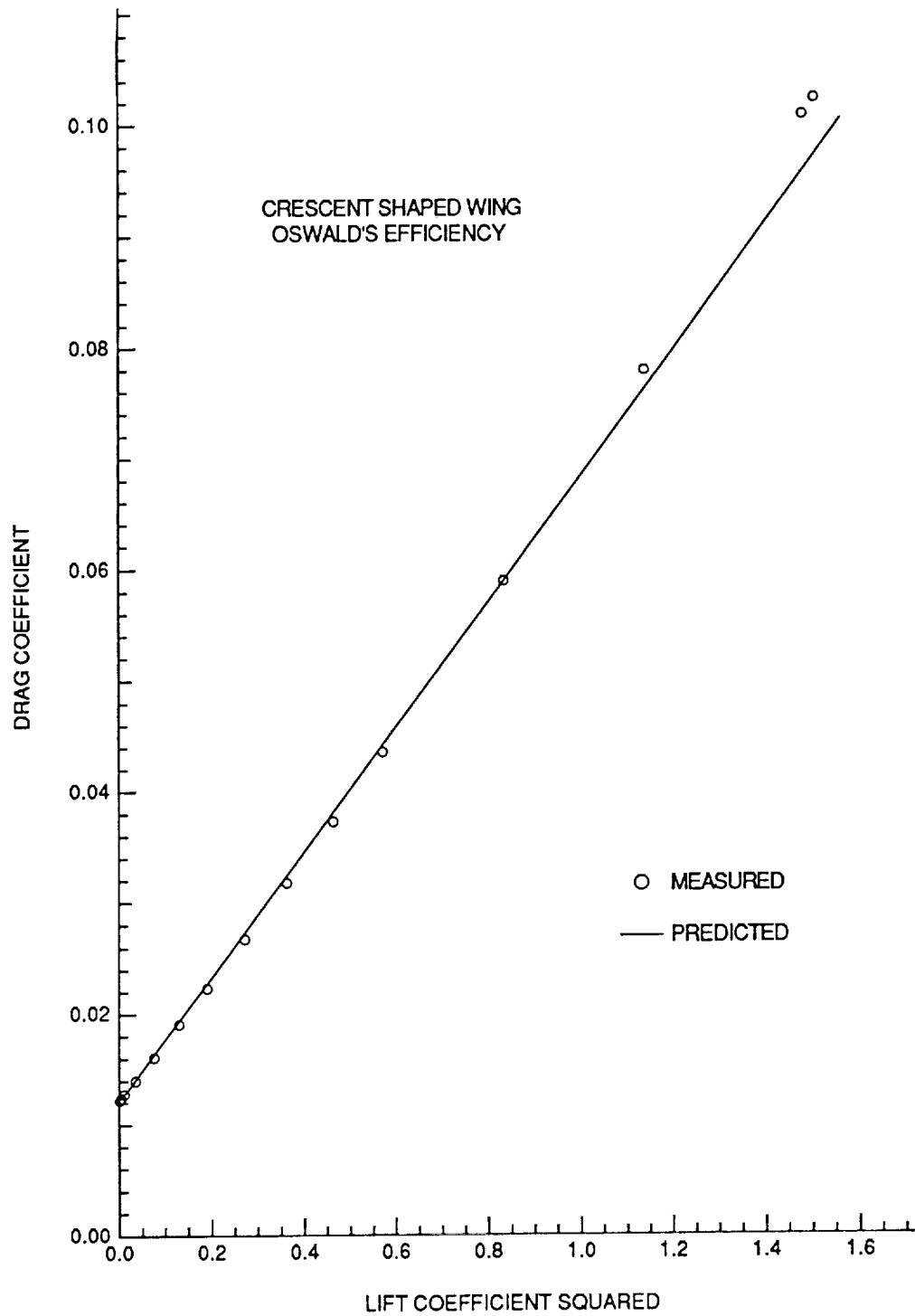


Figure 16: Comparison of the Measured and Predicted Oswald's Efficiencies for the Crescent Shaped Wing

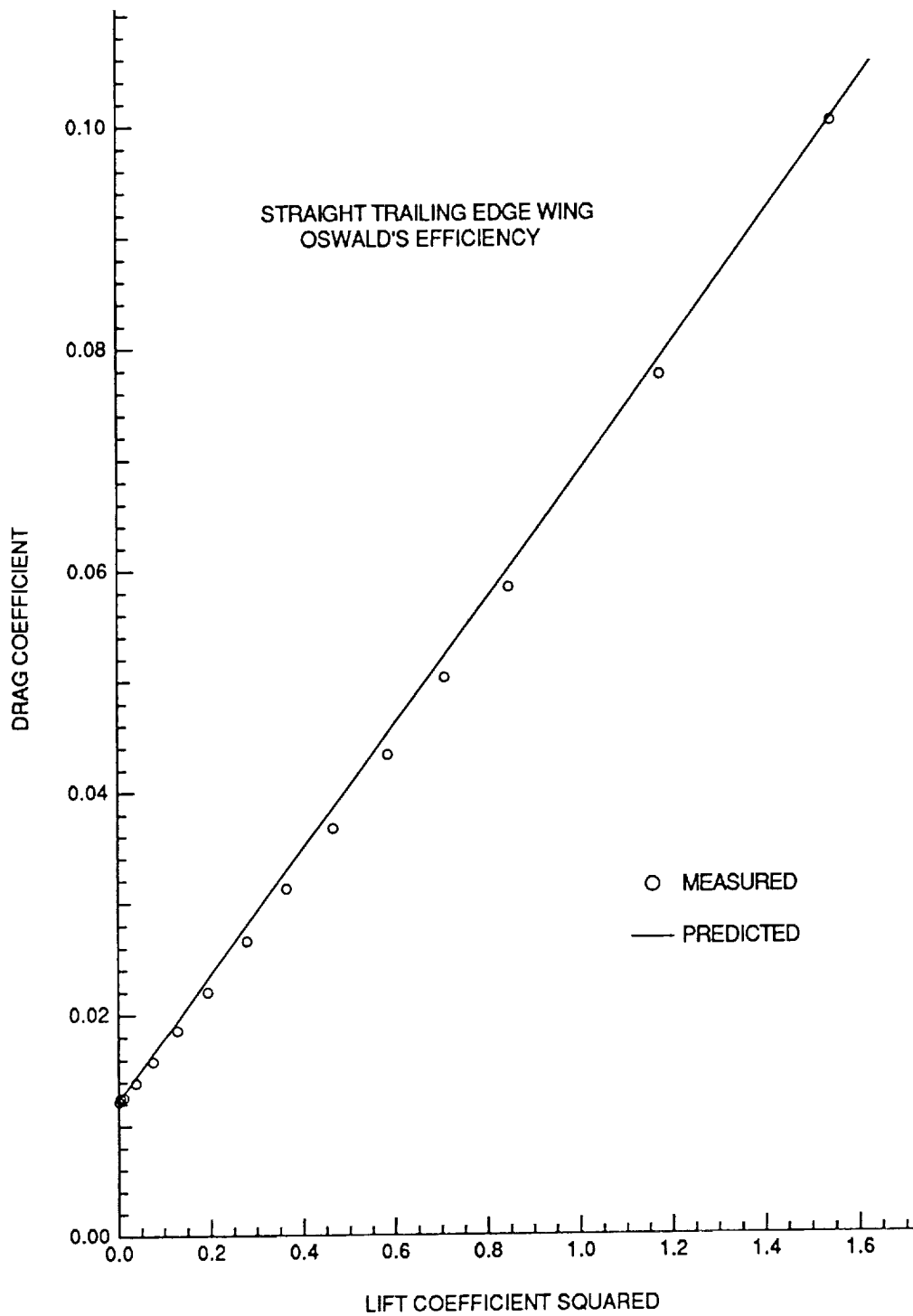


Figure 17: Comparison of the Measured and Predicted Oswald's Efficiencies for the Straight Trailing Edge Wing

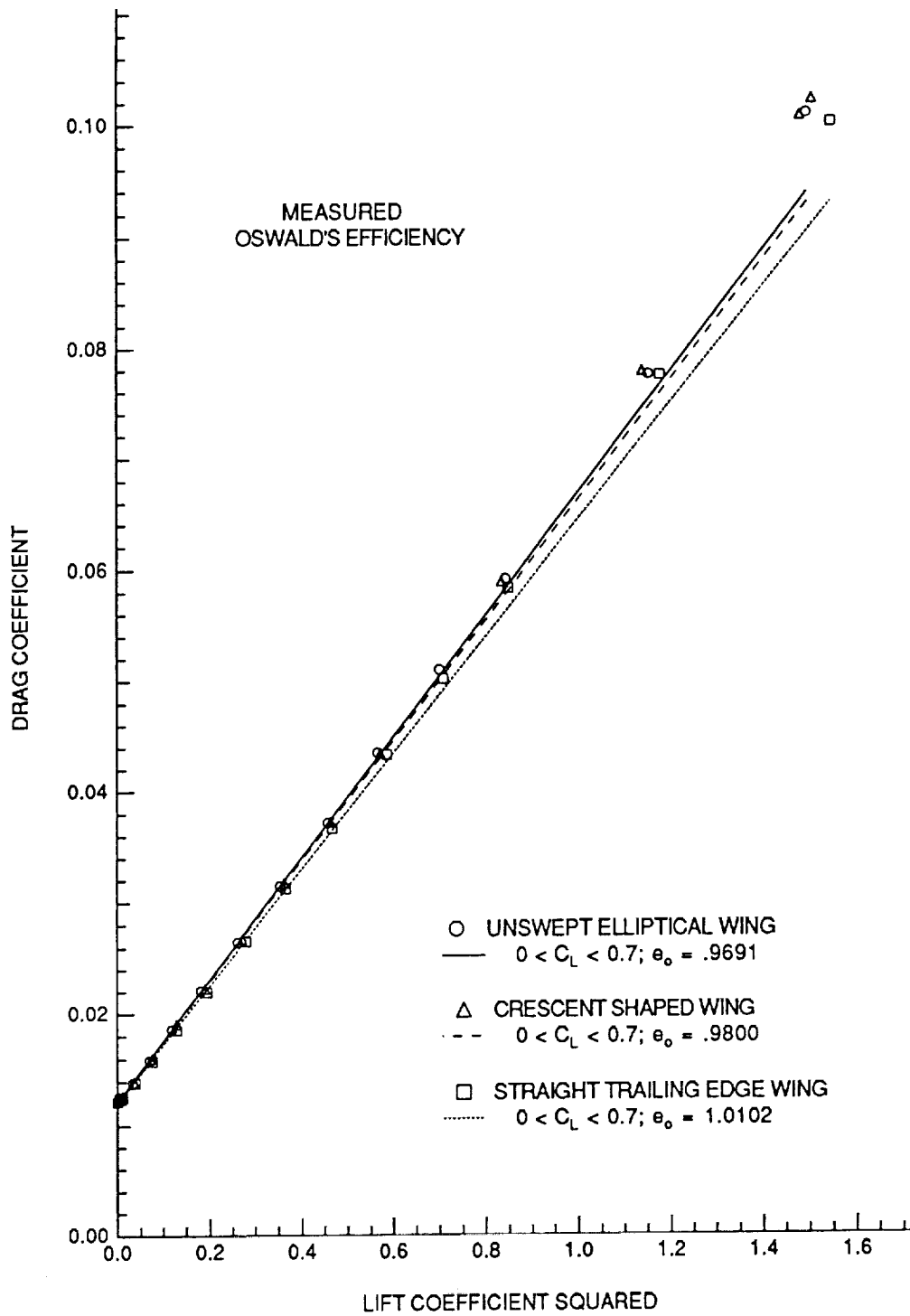


Figure 18: Comparison of the Measured Oswald's Efficiencies of the NASA LaRC Test Wings

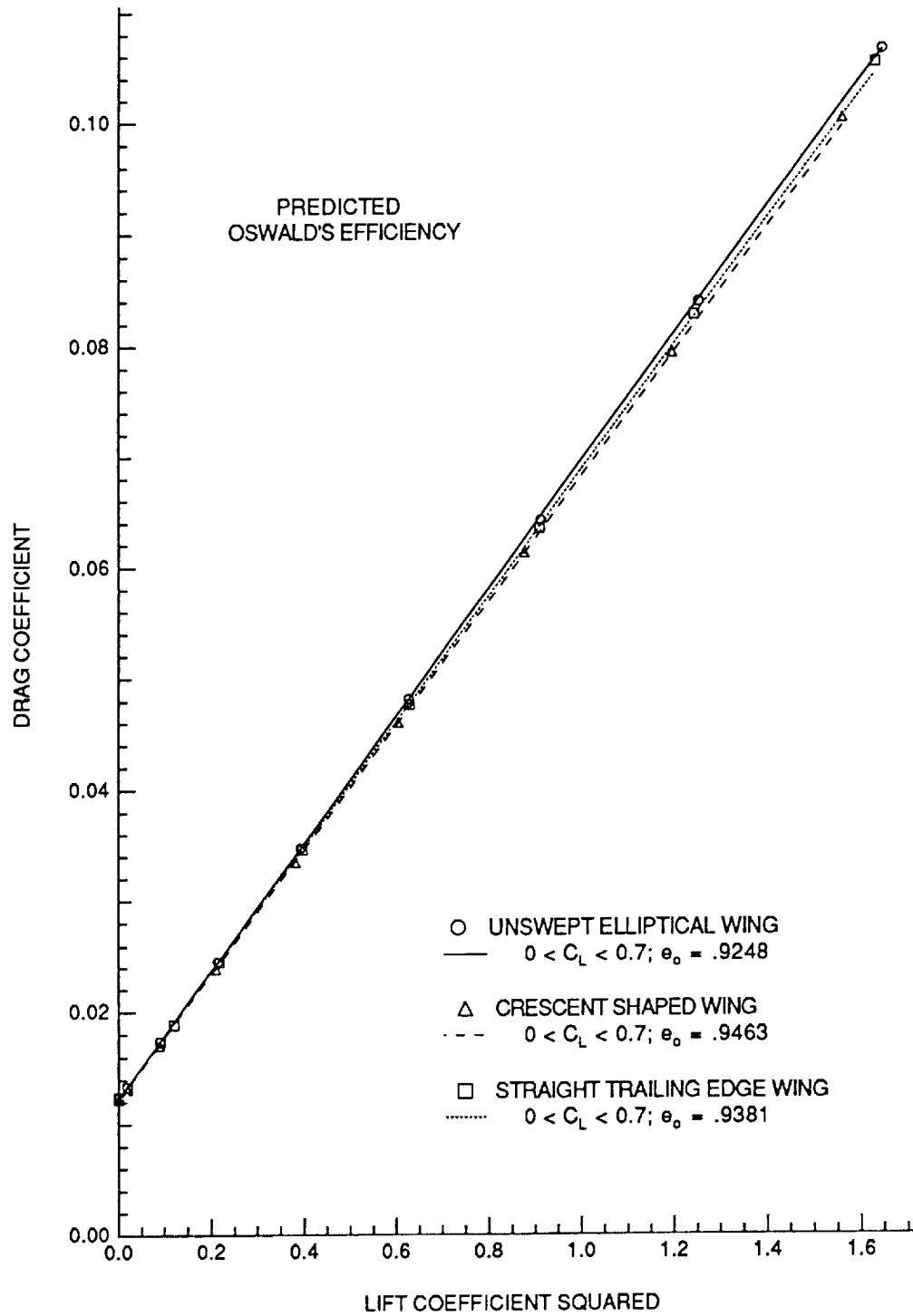


Figure 19: Comparison of the Predicted Oswald's Efficiencies of the NASA LaRC Test Wings

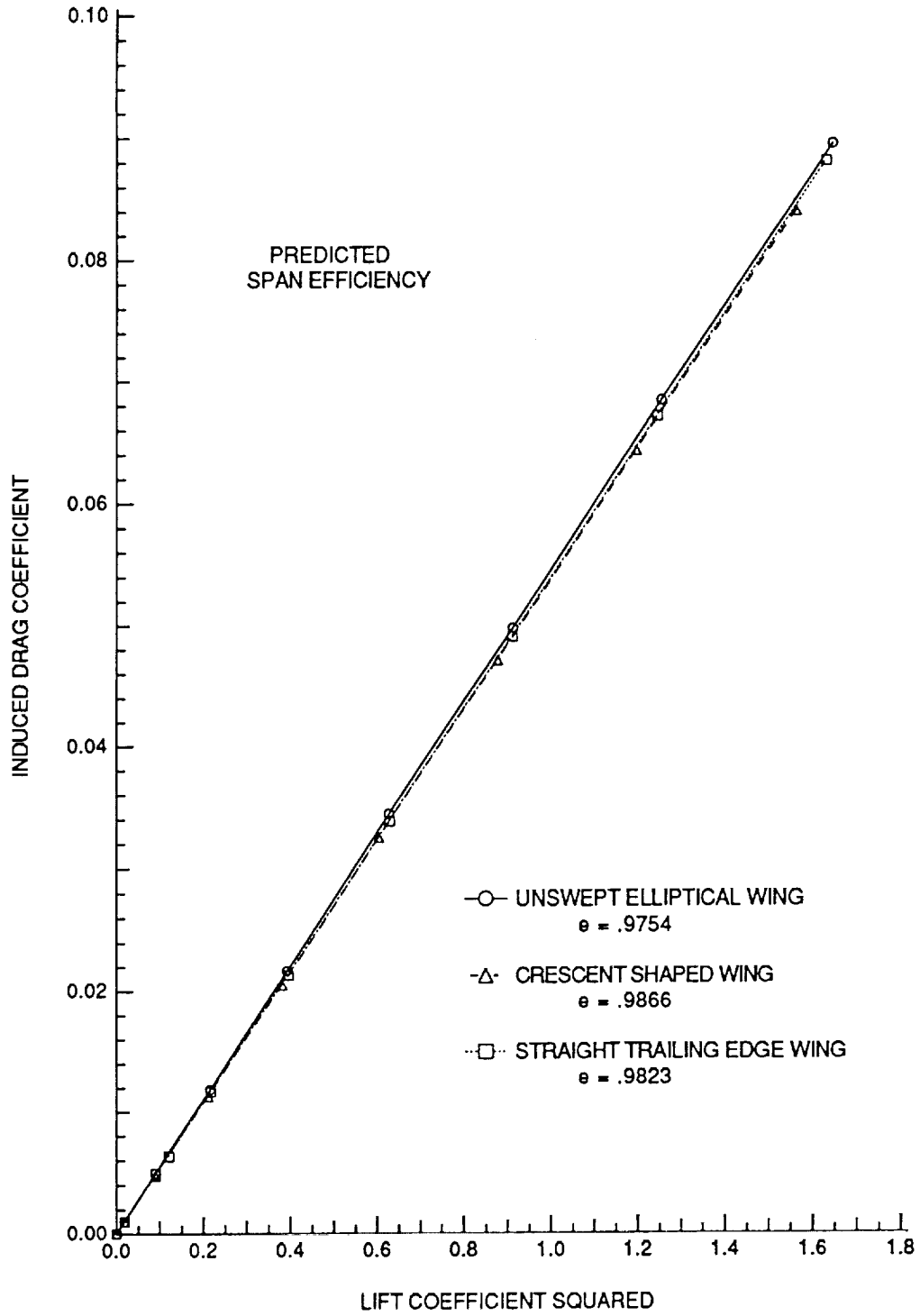


Figure 20: Comparison of the Predicted Span Efficiencies of the NASA LaRC Test Wings

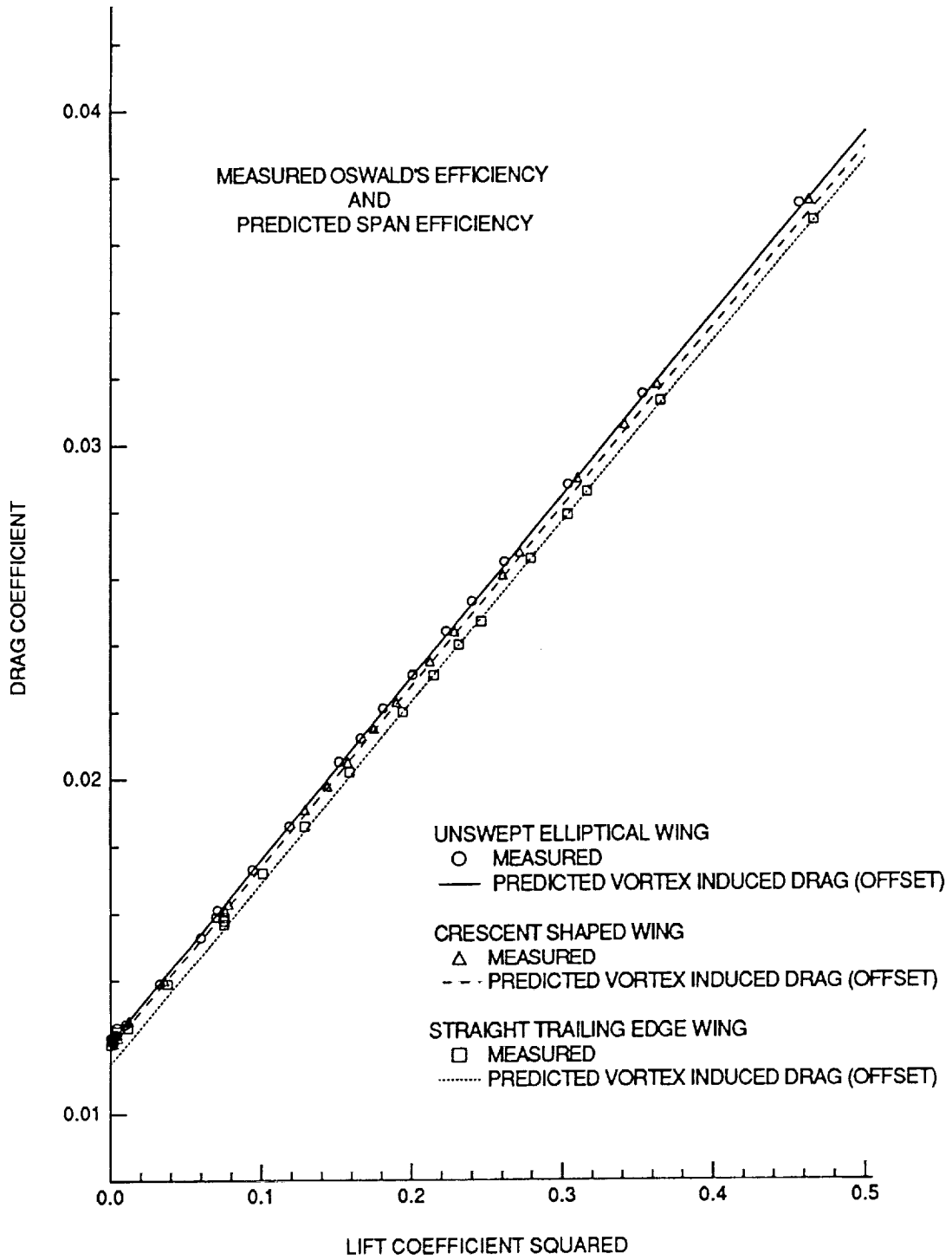


Figure 21: Comparison of Measured Oswald's Efficiency and Predicted Span Efficiency at Low Lift Coefficients for the NASA LaRC Test Wings

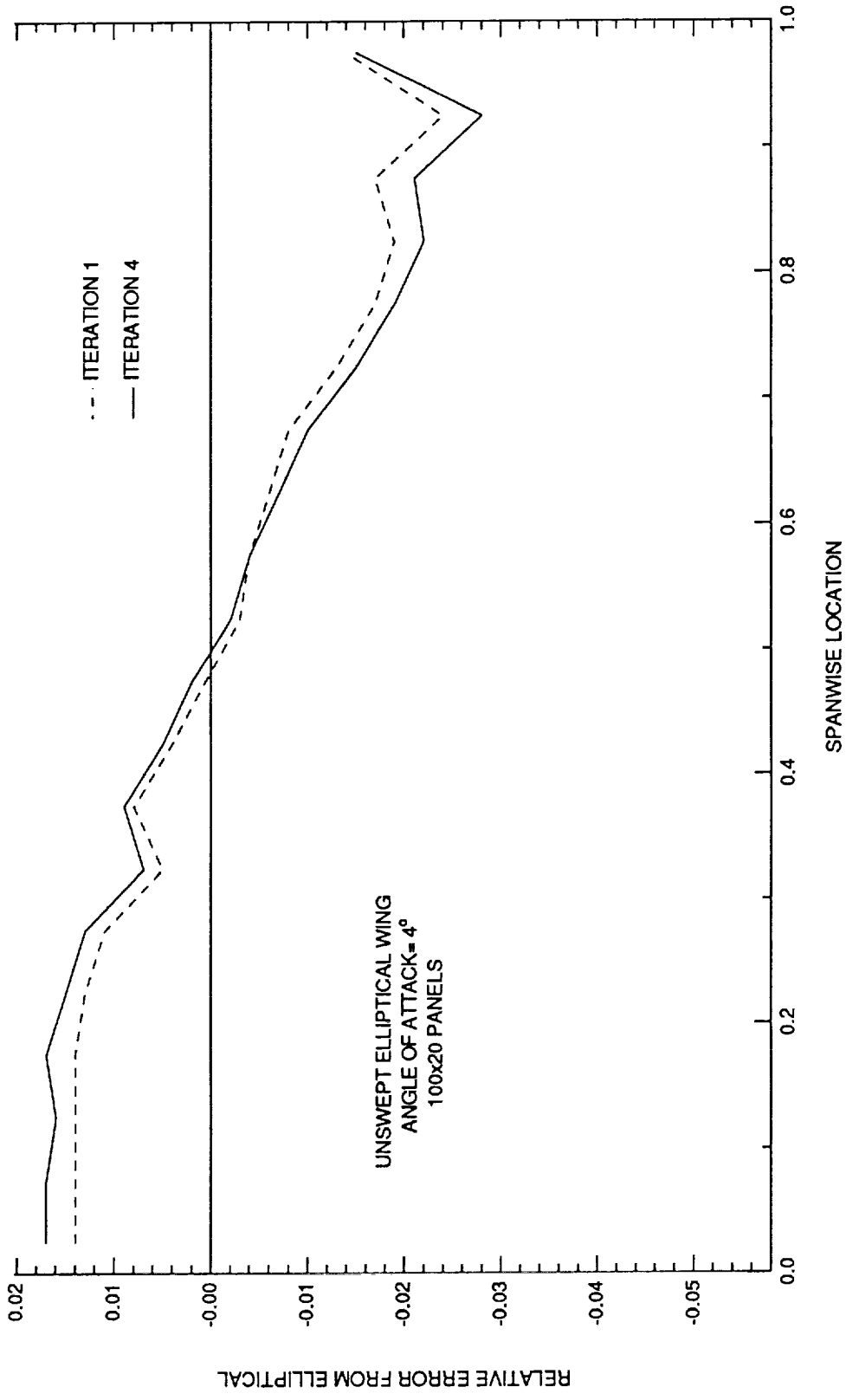


Figure 22: Effect of Wake Deformation on Spanwise Lift Distribution of Unswept Elliptical Wing

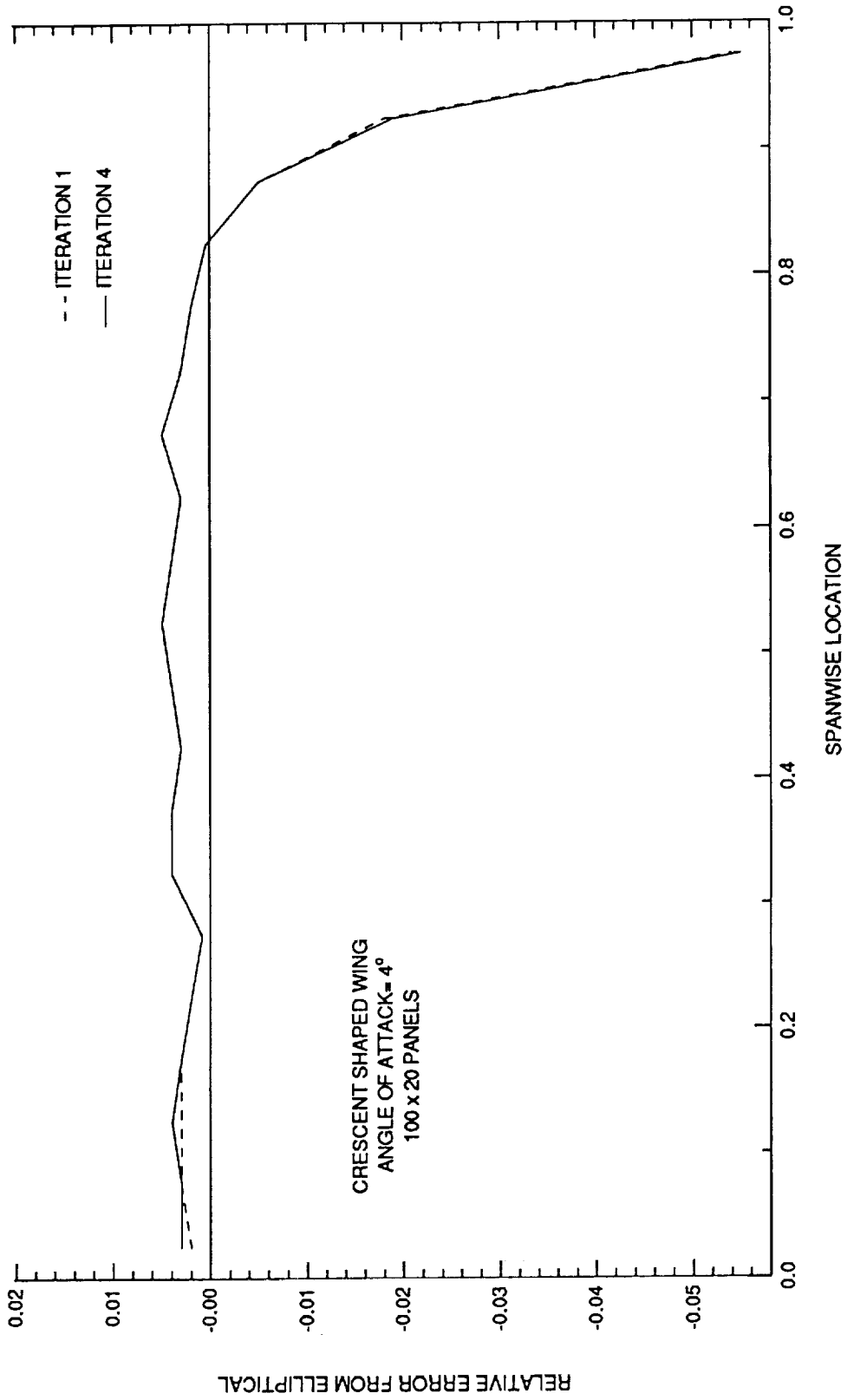


Figure 24: Effect of Wake Deformation on Spanwise Lift Distribution of Crescent Shaped Wing

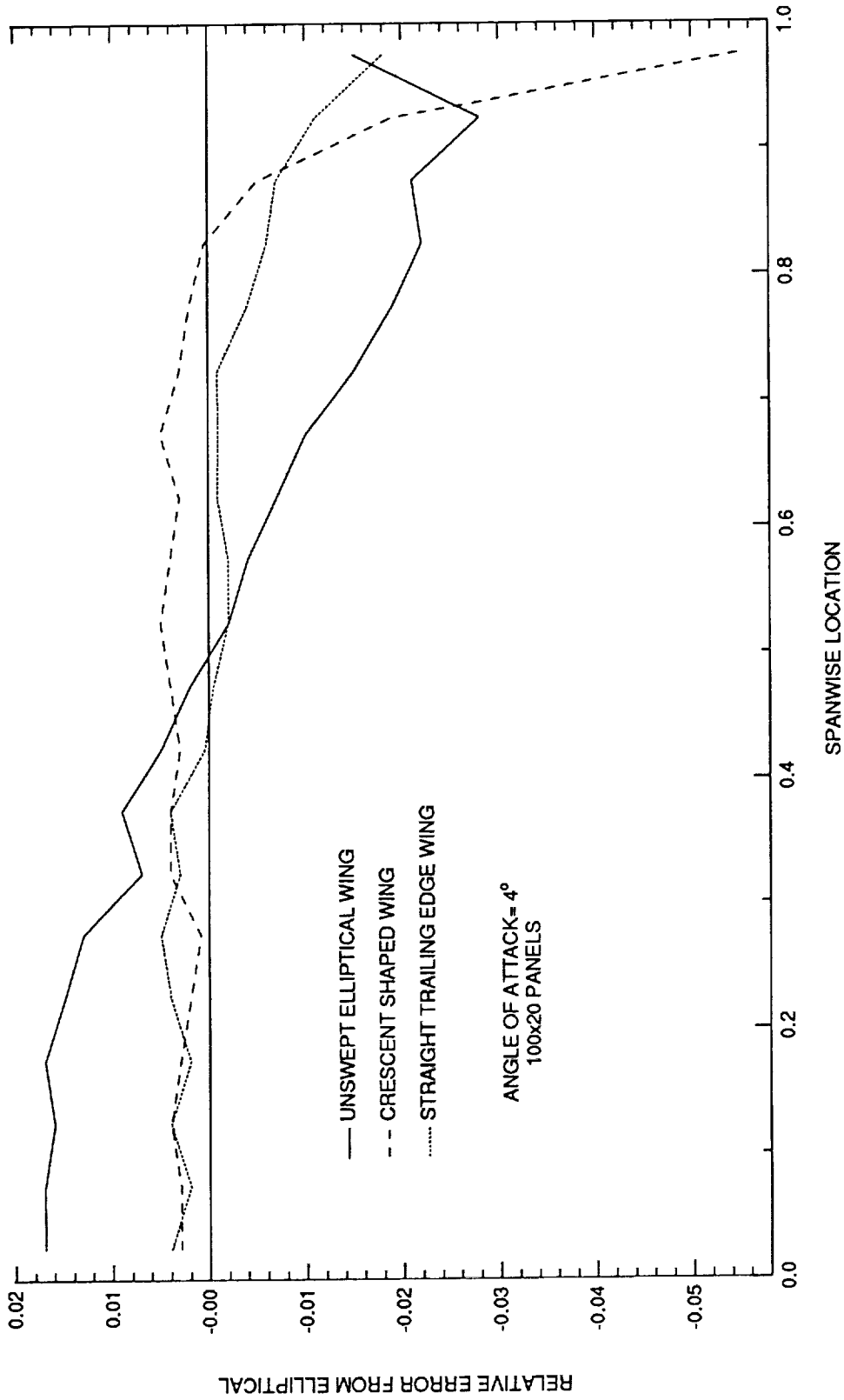


Figure 25: Effect of Wing Tip-Sweep on Spanwise Lift Distribution

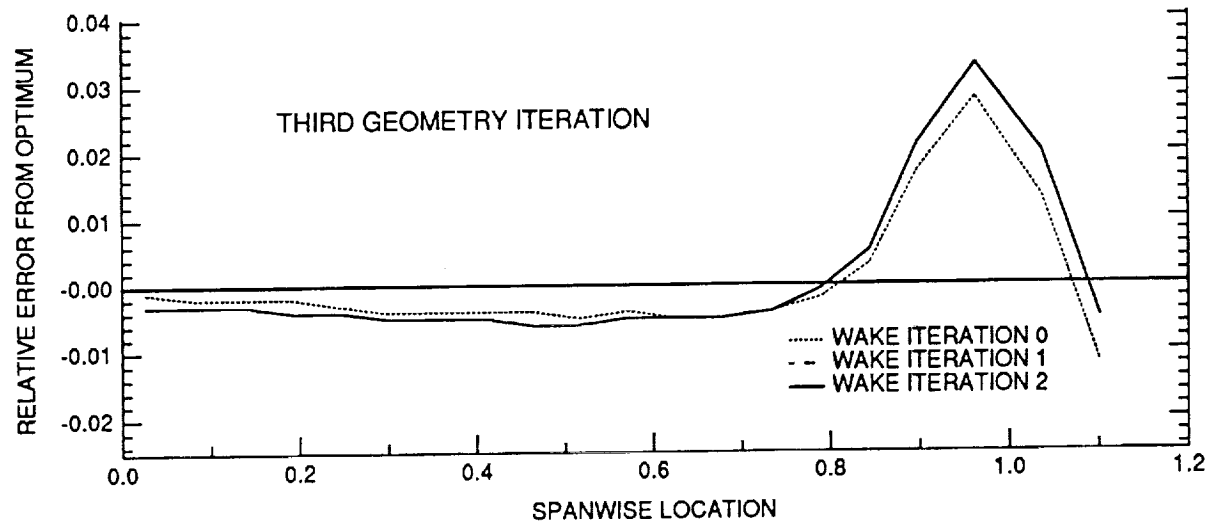
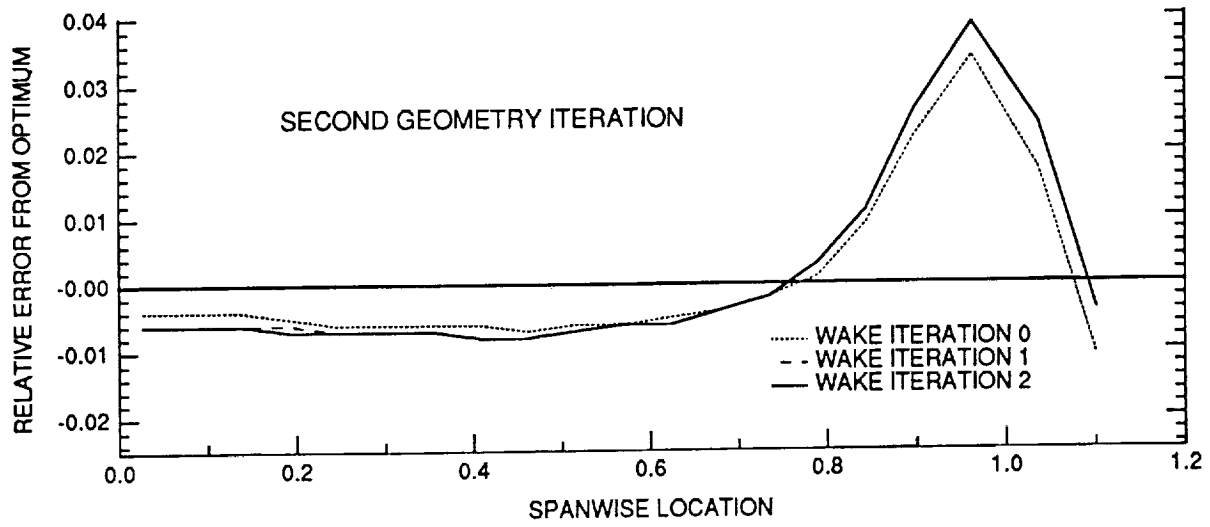
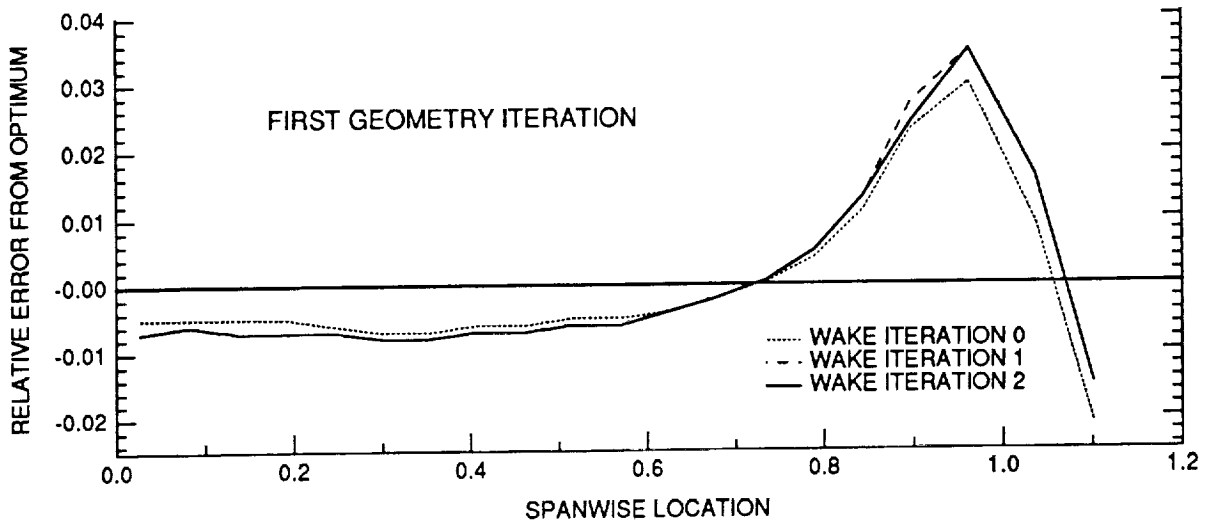


Figure 26: Non-Planar Wing Design Geometry Iterations

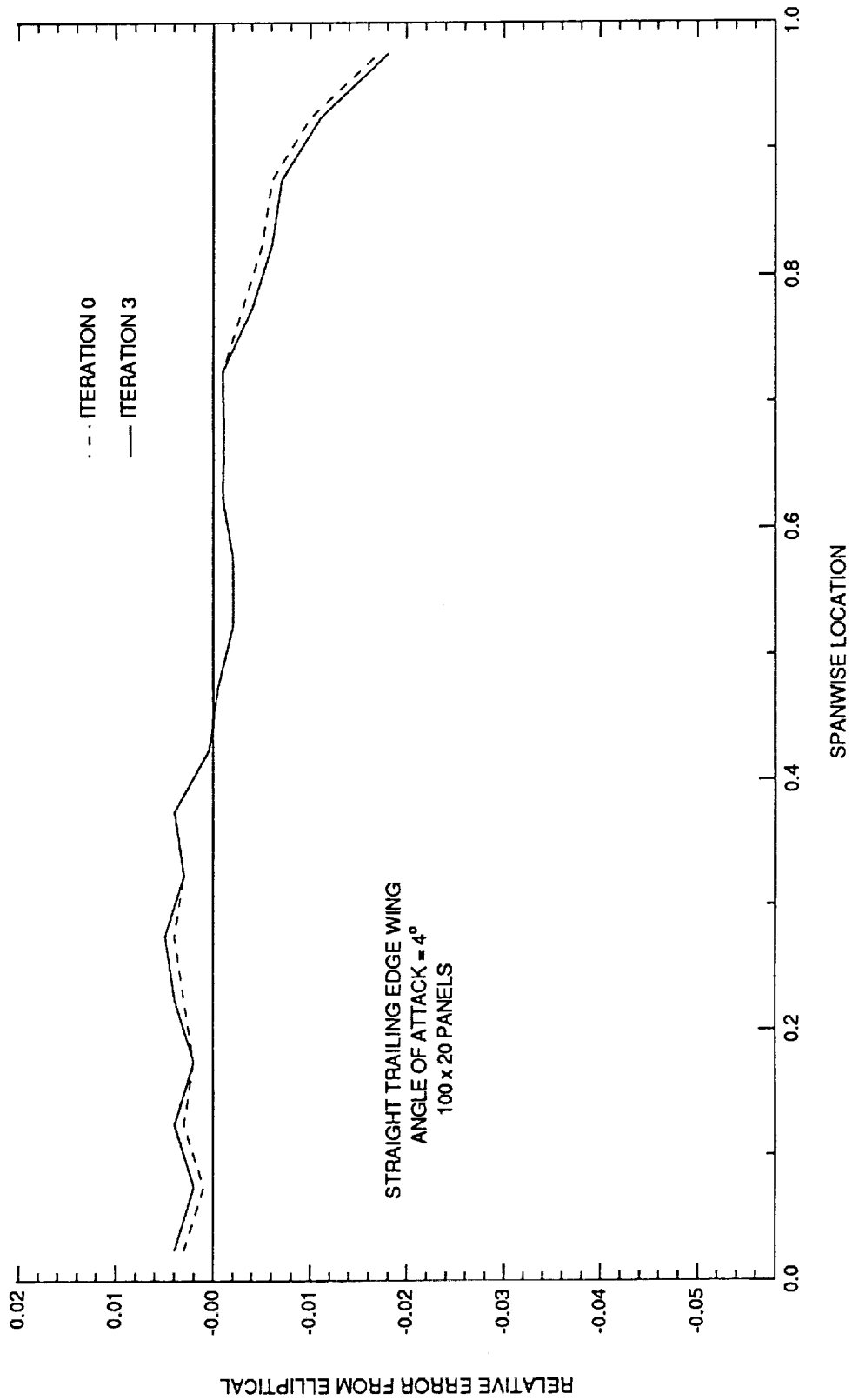


Figure 23: Effect of Wake Deformation on Spanwise Lift Distribution of Straight Trailing Edge Wing